



Observational ozone datasets over the global oceans and polar regions (version 2024)

Yugo Kanaya¹, Roberto Sommariva^{2,3}, Alfonso Saiz-Lopez⁴, Andrea Mazzeo⁵, Theodore K. Koenig^{6,c},
Kaori Kawana^{1,a,b}, James E. Johnson^{7,8}, Aurélie Colomb⁹, Pierre Tulet¹⁰, Suzie Molloy¹¹,
Ian E. Galbally¹², Rainer Volkamer^{13,14}, Anoop Mahajan¹⁵, John W. Halfacre¹⁶, Paul B. Shepson¹⁷,
Julia Schmale¹⁸, Hélène Angot¹⁹, Byron Blomquist¹⁴, Matthew D. Shupe^{20,14}, Detlev Helmig²¹,
Junsu Gil^{22,46}, Meehye Lee²², Sean C. Coburn²³, Ivan Ortega²⁴, Gao Chen²⁵, James Lee^{26,27},
Kenneth C. Aikin^{14,28}, David D. Parrish²⁹, John S. Holloway¹⁴, Thomas B. Ryerson²⁸,
Ilana B. Pollack^{14,28}, Eric J. Williams^{14,28}, Brian M. Lerner³⁰, Andrew J. Weinheimer²⁴,
Teresa Campos²⁴, Frank M. Flocke²⁴, J. Ryan Spackman³¹, Ilann Bourgeois³², Jeff Peischl^{14,28},
Chelsea R. Thompson²⁸, Ralf M. Staebler³³, Amir A. Aliabadi³⁴, Wanmin Gong³³,
Roeland Van Malderen³⁵, Anne M. Thompson³⁶, Ryan M. Stauffer³⁶, Debra E. Kollonige³⁶,
Juan Carlos Gómez Martin³⁷, Masatomo Fujiwara³⁸, Katie Read²⁷, Matthew Rowlinson^{27,16},
Keiichi Sato³⁹, Junichi Kurokawa³⁹, Yoko Iwamoto⁴⁰, Fumikazu Taketani¹, Hisahiro Takashima^{41,1},
Mónica Navarro-Comas⁴², Marios Panagi⁴³, and Martin G. Schultz^{44,45}

¹Japan Agency for Marine-Earth Science and Technology (JAMSTEC), Yokohama, Kanagawa, Japan

²School of Geography, Earth and Environmental Sciences, University of Birmingham, Birmingham, UK

³School of Chemistry, University of Leicester, Leicester, UK

⁴Department of Atmospheric Chemistry and Climate, Institute of Physical Chemistry Blas Cabrera,
CSIC, Madrid, Spain

⁵Lancaster Environment Centre, Lancaster University, Lancaster, UK

⁶State Key Joint Laboratory of Environmental Simulation and Pollution Control, BIC-ESAT and IJRC,
College of Environmental Sciences and Engineering, Peking University, Beijing, China

⁷Cooperative Institute for Climate, Ocean, and Ecosystem Studies,
University of Washington, Seattle, WA, USA

⁸NOAA Pacific Marine Environmental Laboratory, Seattle, WA, USA

⁹LAMP, Laboratoire de Météorologie Physique, UMR 6016, Université Clermont Auvergne,
CNRS, Aubière, France

¹⁰LAERO, Laboratoire d'Aérologie, UMR 5560 CNRS, UT3, IRD, Toulouse, France

¹¹Climate, Atmosphere & Ocean Interactions program, Environment Research Unit,
CSIRO, Aspendale, Victoria, Australia

¹²CSIRO Environment, Aspendale, Victoria, Australia

¹³Department of Chemistry, University of Colorado Boulder, Boulder, CO, USA

¹⁴Cooperative Institute for Research in Environmental Sciences (CIRES),
University of Colorado Boulder, Boulder, CO, USA

¹⁵Centre for Climate Change Research, Indian Institute of Tropical Meteorology, Pashan, Pune, India

¹⁶Wolfson Atmospheric Chemistry Laboratories, Department of Chemistry,
University of York, York, UK

¹⁷School of Marine and Atmospheric Sciences, Stony Brook University, Stony Brook, NY, USA

¹⁸Extreme Environments Research Laboratory, École Polytechnique Fédérale de Lausanne,
EPFL Valais Wallis, Sion, Switzerland

¹⁹Université Grenoble Alpes, CNRS, INRAE, IRD, Grenoble INP, IGE, Grenoble, France

²⁰National Oceanic and Atmospheric Administration, Physical Sciences Laboratory, Boulder, CO, USA

²¹Boulder A.I.R. LLC, Boulder, CO, USA

²²Department of Earth and Environmental Sciences, Korea University, Seoul, Republic of Korea

²³Precision Laser Diagnostics Laboratory, University of Colorado Boulder, Boulder, CO, USA

²⁴NSF National Center for Atmospheric Research, ACOM, Boulder, CO, USA

²⁵NASA Langley Research Center, Hampton, VA, USA

²⁶Department of Chemistry, University of York, York, UK

²⁷National Centre for Atmospheric Science, University of York, York, UK

²⁸NOAA Chemical Sciences Laboratory, Boulder, CO, USA

²⁹David D. Parrish, LLC, Boulder, CO, USA

³⁰Aerodyne Research, Inc., Billerica, MA, USA

³¹NASA Ames Research Center, Moffett Field, CA, USA

³²Université Savoie Mont Blanc, INRAE, CARRTEL, Thonon-les-Bains, France

³³Air Quality Research Division, Science and Technology Branch, Environment and Climate Change Canada, Toronto, ON, Canada

³⁴Department of Mechanical Engineering, College of Engineering, University of Guelph, Guelph, ON, Canada

³⁵Royal Meteorological Institute of Belgium, Uccle (Brussels), Belgium

³⁶NASA Goddard Space Flight Center, Greenbelt, MD, USA

³⁷Instituto de Astrofísica de Andalucía, Consejo Superior de Investigaciones Científicas, Granada, Spain

³⁸Faculty of Environmental Earth Science, Hokkaido University, Sapporo, Japan

³⁹Asia Center for Air Pollution Research, Niigata, Niigata, Japan

⁴⁰Graduate School of Integrated Sciences for Life, Hiroshima University, Higashi-Hiroshima, Japan

⁴¹Faculty of Science, Fukuoka University, Fukuoka, Japan

⁴²Atmospheric Research and Instrumentation Branch, National Institute for Aerospace Technology (INTA), Madrid, Spain

⁴³Climate and Atmosphere Research Center, The Cyprus Institute, Nicosia, Cyprus

⁴⁴Jülich Supercomputing Center, Forschungszentrum Jülich GmbH, Jülich, Germany

⁴⁵Department of Mathematics and Computer Science, University of Cologne, Cologne, Germany

⁴⁶Institute of Basic Sciences, Korea University, Seoul, Republic of Korea

^anow at: Institute of Chemical Engineering Sciences, Foundation for Research and Technology – Hellas (FORTH/ICE-HT), Patras, Greece

^bnow at: School of Architecture, Civil and Environmental Engineering, École Polytechnique Fédérale de Lausanne (EPFL), Lausanne, Switzerland

^cnow at: Division of Environment and Sustainability, The Hong Kong University of Science and Technology, Hong Kong SAR, China

Correspondence: Yugo Kanaya (yugo@jamstec.go.jp)

Received: 28 November 2024 – Discussion started: 13 February 2025

Revised: 24 May 2025 – Accepted: 28 May 2025 – Published: 26 September 2025

Abstract. Studying tropospheric ozone over the remote areas of the planet, such as the open oceans and the polar regions, is crucial to understand the role of ozone as a global climate forcer and regulator of atmospheric oxidative capacity. A focus on the pristine oceanic and polar regions complements the available land-based datasets and provides insights into key photochemical and depositional loss processes that control the concentrations and spatiotemporal variability in ozone as well as the physicochemical mechanisms driving these patterns. However, an assessment of the role of ozone over the oceanic and polar regions has been hampered by a lack of comprehensive observational datasets. Here, we present the first comprehensive collection of ozone data over the oceans and the polar regions. The overall dataset consists of 77 ship cruises/buoy-based observations and 48 aircraft-based campaigns. The dataset, consisting of more than 630 000 independent ozone measurement data points covering the period from 1977 to 2022 and an altitude range from the surface to 5000 m (with a focus on the lowest 2000 m), allows systematic analyses of the spatiotemporal distribution and long-term trends over the 11 defined ocean/polar regions. The datasets from ships, buoys, and aircraft are complemented by ozonesonde data from 29 launch sites or field campaigns and by 21 non-polar and 17 polar ground-based station datasets. The datasets contain information on how long the observed air masses were isolated from land, as estimated by backward trajectories from the individual observation points. To extract observations representative of oceanic conditions, we recommend using a subset of the data with an isolation time of 72 h or longer, from the analysis with coincident radon observations. These filtered oceanic and polar data showed typically flat diurnal cycles at high

latitudes, whereas daytime decreases in ozone (11 %–16 %) were observed at lower latitudes. The ship/buoy- and aircraft-based datasets presented here will supplement the land-based ones in the TOAR-II (Tropospheric Ozone Assessment Report Phase II) database to provide a fully global assessment of tropospheric ozone. The described dataset is available at <https://doi.org/10.17596/0004044> (Kanaya et al., 2025).

1 Introduction

As a short-lived species with an estimated lifetime of 25.5 ± 2.2 d (Griffiths et al., 2021; Szopa et al., 2021), both global/hemispheric and regional/local aspects need to be emphasized in the assessment of tropospheric ozone. While the spatiotemporal variation over land is primarily important for assessing vegetation and health impacts, its behavior over the oceans is critical when assessing its climate impact as the third most important greenhouse gas (Forster et al., 2021). The role of ozone in maintaining the global oxidative capacity of the atmosphere through the production of the OH radical also requires understanding on a global scale. The overall budget of tropospheric ozone is dominated by the photochemical production and loss terms, estimated at 4500–5000 and 3900–4500 Tg yr⁻¹, respectively, rather than by the stratosphere–troposphere exchange (270–540 Tg yr⁻¹) or surface deposition (800–1000 Tg yr⁻¹) for decades around 2000 or 2010 (Griffiths et al., 2021; Young et al., 2018). The net ozone production mainly occurs over regions with NO_x pollution and depends on the abundance of volatile organic compounds (VOCs). By contrast, the net loss conditions, which are driven by OH/HO₂ radical chemistry in a low-NO_x environment and potentially also by understudied halogen chemistry, occur mostly over remote regions, including over the oceans (Galbally et al., 2000; Monks et al., 1998; Stone et al., 2018; Read et al., 2008; Dickerson et al., 1999; Boylan et al., 2015; Saiz-Lopez and von Glasow, 2012; Simpson et al., 2015). Another important loss term is from dry deposition on the ocean surface, which depends on the chemical composition of the surface seawater and its physical conditions (Helmig et al., 2012; Hardacre et al., 2015; Ganzeveld et al., 2009; Pound et al., 2020; Sarwar et al., 2016; Luhar et al., 2018; Barten et al., 2023; Chiu et al., 2024) and which has not been fully characterized. Therefore, there is a special need to study the ozone concentration levels and spatiotemporal variations as well as the underlying mechanisms that control ozone levels over the oceans. However, observational data of ozone over oceanic regions are much less abundant than those over the land, preventing a full assessment. TOAR (Tropospheric Ozone Assessment Report) is an IGAC (International Global Atmospheric Chemistry project)-sponsored activity which aims to collect ozone observations in the troposphere. At the time of TOAR-I (Schultz et al., 2017), oceanic data were collected only from island-based surface monitoring observations and ozoneson-

des, with some satellite-based information, but the oceanic regions remained devoid of data.

The polar regions are other pristine areas, with episodic ozone destruction in the polar sunrise season (Simpson et al., 2007). During the International Polar Year 2007–2008, extensive studies on ozone were conducted and published and published in the POLARCAT (Polar Study using Aircraft, Remote Sensing, Surface Measurements and Models, of Climate, Chemistry, Aerosols, and Transport) special issue (ACP, 2015). An assessment report on short-lived climate forcers from the Arctic Council's Arctic Monitoring and Assessment Programme (AMAP, 2021) and synthesis papers (Whaley et al., 2023; Law et al., 2023) have recently been produced, but comprehensive studies based on multi-platform observations are still lacking.

To improve the situation, a working group on ozone over the oceans and the polar regions (Oceans working group) has been formed within the TOAR-II activity to provide a comprehensive dataset, especially with ship-, buoy-, and aircraft-based observations over the oceans, to allow a first assessment over the entire ocean area and polar regions. In the past, studies on ozone over the oceans were conducted using ship-based/aircraft-based ozone observations, but they were mostly based on observations from a single campaign/series of related campaigns (e.g., Dickerson et al., 1999; Bourgeois et al., 2020) or, at best, from a collection of observations from a single nation/project (e.g., Lelieveld et al., 2004; Kanaya et al., 2019); here we aim to collect data from multiple nations, research groups, and campaigns to achieve a better global coverage, using the IGAC framework as a global research network (GRN) of Future Earth, on which the TOAR activity is based. The resulting five datasets include observations from ships/buoys, aircraft, ozonesondes, ground-based coastal/island sites, and polar stations. This data paper primarily describes two of these datasets, which consist of 77 ship- or buoy-based observations and 48 aircraft observations over the global oceans and polar regions covering a period between 1977 and 2022. The altitude range covered by the data is from the surface to 5000 m, with a focus on the lowest 2000 m, as a major interest of the working group lies within the atmospheric boundary layer, where the interfacial interactions of the atmosphere with the ocean and snow/ice surfaces (even including biogeochemical processes), as well as the photochemistry, are of particular relevance. A third dataset contains ocean and polar ozonesonde data, mostly obtained from coastal/island sonde launching sites. The ozonesonde data were mainly

provided by the HEGIFTOM (Harmonization and Evaluation of Ground-based Instruments for Free-Tropospheric Ozone Measurements) Focus Working Group of the TOAR-II activity and, therefore, include their data homogenization procedure (Van Malderen et al., 2025), but they were further processed by the Oceans working group here. These three datasets are complemented by two datasets containing ground-based data from coastal/island sites and from polar stations, selected from the TOAR-II database (Schröder et al., 2024) with some additional field campaign sites. Satellite data are not included in this study because they are discussed elsewhere in the TOAR-II special issue (Gaudel et al., 2024; Pope et al., 2023) and because it is still difficult to resolve the commonly low ozone levels in the boundary layer over the oceans from satellite observations.

The result of this work enables integrated studies of the long-term and/or seasonal trends from ship-based observations and established coastal-site observations in the same region, for example, at Cabo Verde, Kennaook/Cape Grim, Mace Head, and Trinidad Head (e.g., Parrish et al., 2009). To be suited for the ocean-focused studies, all five datasets are complemented with information on how many hours each observed air mass was separated from land, derived from backward trajectories. Note that a full assessment of tropospheric ozone in the remote regions (oceans and polar) using these datasets will be published separately (Sommariva et al., 2025) as part of the TOAR-II series of assessment papers; here, we focus on the data description, including its preparation and harmonization.

2 Data description

The overall geographical distribution of the collected ship/buoy data, aircraft-based data (up to 5000 m but considering 0–2000 m altitude as a key part for the study of the boundary layer), and selected ozonesonde/surface observation sites is shown in Fig. 1. The following subsections describe each dataset in detail. The data are divided into 11 regions (2 polar and 9 oceanic). Following the recommendation of the TOAR-II Steering Committee (TOAR-II Steering Committee, 2023), the regions are broadly defined as follows: polar ($60\text{--}90^\circ\text{ N}$ and $90\text{--}60^\circ\text{ S}$), midlatitude ($20\text{--}60^\circ\text{ N}$ and $60\text{--}20^\circ\text{ S}$), and tropical ($20^\circ\text{ S}\text{--}20^\circ\text{ N}$). The boundaries are adjusted by 4° or less to take into account geography or the position of the land masses (Fig. 1). The Pacific sector (from $100\text{--}115^\circ\text{ E}$ to $100\text{--}69^\circ\text{ W}$, across the International Date Line) is subdivided into northern (R1; $22\text{--}63^\circ\text{ N}$), tropical (R2; $20^\circ\text{ S}\text{--}22^\circ\text{ N}$), and southern (R3; $60\text{--}20^\circ\text{ S}$) regions. The Indian Ocean (from $20\text{--}34^\circ\text{ E}$ to $100\text{--}115^\circ\text{ E}$) is divided into tropical (R4; $20^\circ\text{ S}\text{--}31^\circ\text{ N}$) and southern (R5; $60\text{--}20^\circ\text{ S}$) regions. The eastern part of the Mediterranean Sea and the Black Sea ($15\text{--}55^\circ\text{ E}$, $31\text{--}59^\circ\text{ N}$) are given a code R6, but we did not collect data from these areas because continental influences were generally unavoidable. The Atlantic sector

(from $100\text{--}69^\circ\text{ W}$ to $15\text{--}20^\circ\text{ E}$) is divided into northern (R7; from $16\text{--}23^\circ\text{ E}$ to 62° N), tropical (R8; $20^\circ\text{ S}\text{--}23^\circ\text{ N}$, including the Caribbean), and southern (R9; $60\text{--}20^\circ\text{ S}$) regions. The Arctic region (R10) is defined as north of $59\text{--}63^\circ\text{ N}$ (depending on the longitude) and the Antarctic region (R11) as south of 60° S .

2.1 Ship/buoy dataset

A total of 208 291 hourly averaged ozone concentration data were collected from 62 ship cruises (or aggregated cruises/legs) and from 15 buoy operations and archived in the file `toar2_oceans_ship_buoy_data_250203.csv`, covering the 1977–2022 period (Table 1, Fig. 1). The data come from research groups in the USA, Japan, Australia, Germany, France, Switzerland, Spain, India, and the Republic of Korea. The instruments used are mainly research-grade ozone monitors based on UV absorption, with the exception of the DWD-MPI (Deutscher Wetterdienst – Max Planck Institute) dataset before 1996 which employed a wet chemical instrument using the potassium iodide (KI) method. The ship's exhaust plume could affect all of the cruise observations, depending on the relative wind directions with respect to the ship's funnel and the inlet position of the gas sampling tube. A fast-response ozone monitor could easily detect such cases of pollution, as NO in the exhaust titrates the atmospheric ozone quickly. The buoy measurements do not have the risk of a plume effect; therefore, their hourly averages were constructed from the original 10 s raw data without filtering to preserve the real ozone reduction episodes over the Arctic region.

The ship datasets were processed as follows. First, minute data below the hourly mean minus 1σ were removed. Following this, hourly averages were recalculated. The hourly data were removed if the variability in the valid minute data was greater than 10 % of the hourly mean. This two-step filtering procedure is similar to Kanaya et al. (2019) and was found to be suitable to remove the ship's influence in different cruise datasets. Figure S1 in the Supplement shows a case of flagging and data removal from the time series of the R/V *Hakuho Maru* cruise KH18-6. Filtering was applied to cruises for which 1 min resolution data were available, i.e., R/V *Mirai* cruises during 2012–2021 (MR 12–21), *Hakuho Maru* KH-18-6, NAAMES1–4, ATOMIC, DYNAMO, WACS, VOCALS, NEAQS 2002, NEAQS 2004, TEXAQS 2006, ICEALOT, CalNex 2010, DRAKE2009, IN MAP-IO (SWINGS 2021, OP1 TAAF 2021, SCRATCH 2021, OP2 TAAF 2021, MAYOBS 2021, OP3 TAAF 2021, and OP4 TAAF 2021; http://173.249.47.189/new_mapio_web/home/, last access: 6 September 2025), *Ka'imimoana*, 17v01-05, 18v01-06, 08, 19v01-03, IIQE2, SOE9, and SOE11. The original data from MAGE92, RITS93, RITS94, ACE1, AEROSOLS99-INDOEX, and ACE-Asia were on a 30 min basis and were averaged to an hourly resolution. The original hourly data

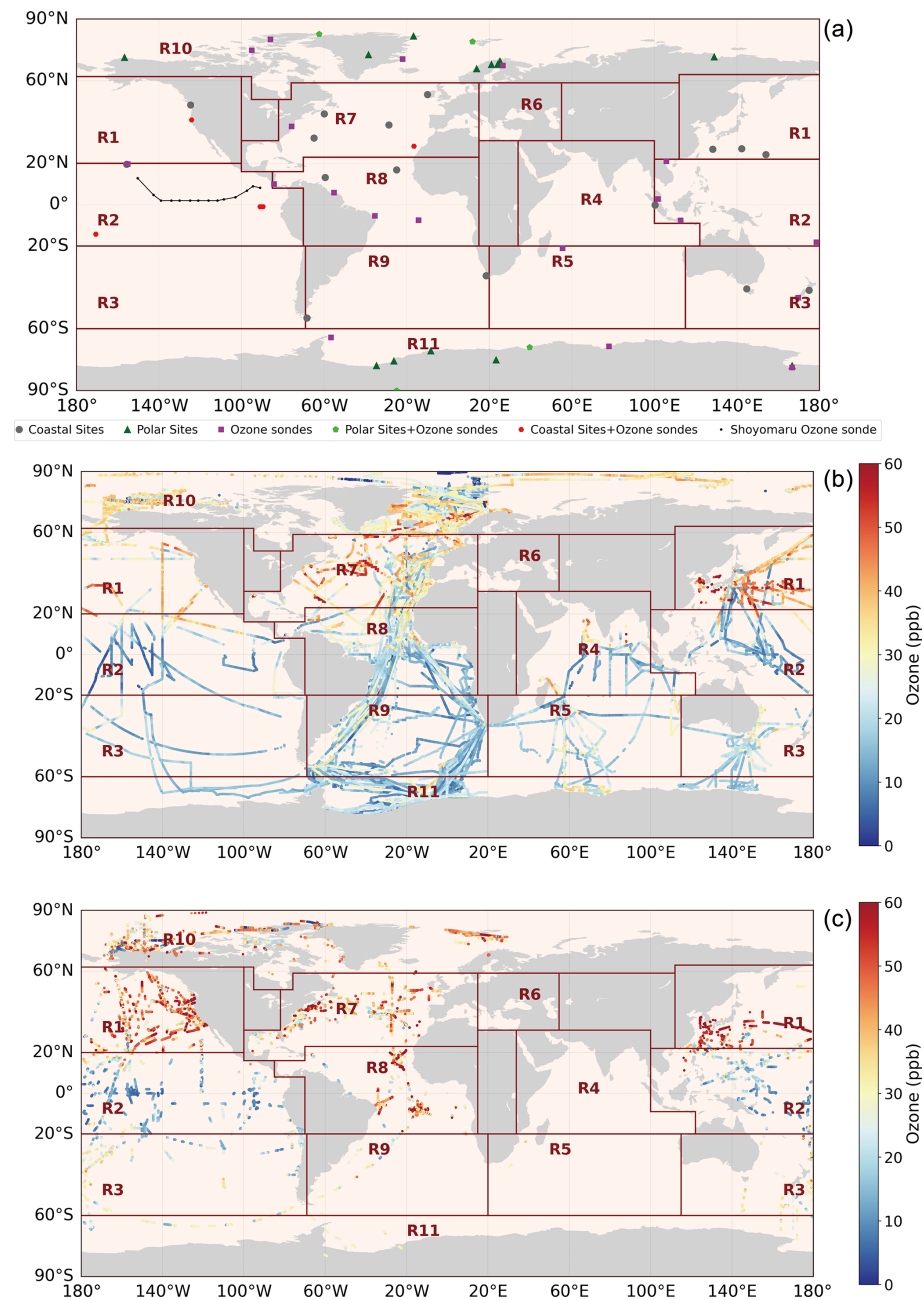


Figure 1. Locations of ozonesonde and coastal/polar ground observations (a). Overall ship/buoy ozone data (b) and airborne ozone data with altitudes < 2000 m (c) after filtering for $LCL \geq 72$ h. Ozone levels above 60 ppb are omitted for clarity.

from Malaspina, SAGA3, DWD-MPI, YES-AQ, and MOSAiC were used as they were provided. We assumed that basic quality control had been performed (e.g., see Angot et al., 2022, for the MOSAiC dataset). The DWD-MPI data are a large compilation of 51 cruises with different research vessels (*Meteor*, *Polarstern*, *Walther Herwig*, *Anton Dohrn*, *Ymer*, and *Academie Fedorov*) collected by Deutscher Wetterdienst (DWD) in the 1977–1996 period, 27 cruises with the container ship *Berlin Express* collected by Max Planck Institute (MPI) in the 1995–2002 period, and one *Meteor*

cruise conducted by MPI in 2002, with a clear note that the data have been screened for local influences of the research vessel itself and of nearby passing ships and that data in and near harbors and in channels have been removed.

Some cruises included additional observations of pollution tracers, i.e., CO, NO, NO₂, and condensation nuclei (CN) with diameters larger than 11–13 nm, and these data are archived together with ozone (see Table 1 and Table S1 in the Supplement for the observation methods and uncertainties). However, the tracer observations did not cover the entire

dataset and, therefore, could not be used uniformly for further systematic screening of air masses influenced by pollution arising from nearby land (even if present). It is an essential requirement of oceanic ozone studies to be able to distinguish between air masses representing the remote ocean and those influenced by pollution from nearby land. Therefore, we calculated backward trajectories for each hourly dataset to add information on the “last contact with land” (LCL, in the unit of hours ago), as a semi-quantitative index indicating how long the air masses were isolated from a land region with potential pollution before the observations. The land mask data from NASA (NASA, 2019) with a resolution of 0.25° were used. The high-latitude regions ($65\text{--}90^\circ\text{N}$ or $90\text{--}60^\circ\text{S}$) were not considered to be “land”, and the land mask was assumed only up to an altitude of 2500 m, as the pollution effect from land would be minimal at higher altitudes. Exceptions may include lifted plumes, such as those from biomass burning. The 2500 m threshold is tentative in an attempt to yield a criterion that is meaningful for the entire globe. It may be revisited after detailed analysis in the assessment. Backward trajectories were computed with the HYSPLIT version 4 model (Draxler and Rolph, 2013) using 6-hourly GDAS1 ($1 \times 1^\circ$) meteorological fields after December 2004 or using 6-hourly NCEP/NCAR Reanalysis product (RP{YEAR}{MONTH}.bgl) files with a 2.5° resolution for the earlier period. Harris et al. (2005) studied the uncertainty in the trajectories using the NCEP/NCAR Reanalysis product. The starting altitude for ship/buoy observations was set to 500 m and the duration to 120 h. The first point of land contact was marked to provide the LCL information. An LCL value of 120 h was assigned to the air masses if no land contact occurred for the entire period.

We defined a criterion of $\text{LCL} \geq 72\text{ h}$ (hereafter referred to as LCL72) to identify marine air masses that have been minimally influenced by land. Figure 2 shows examples of the backward trajectories calculated for the MR19-03C cruise between Japan and the Arctic and for the RITS94 cruise from North to South America, respectively. The light-blue and purple lines represent trajectories for marine and land-influenced air mass cases, respectively. The red lines indicate the cases in which the observed ozone mixing ratio was greater than 50 ppb (polluted).

The LCL72 criterion was evaluated using observed radon concentrations from ACE-1 (Whittlestone et al., 1998), ACE-Asia, ATOMIC, ICEALOT, NAAMES1–4, and WACS shipborne observations as a tracer of land contact (Fig. 3). Radon, emitted from land and lost with a half-life of 3.8 d (Zhang et al., 2021), is suitable for testing the performance of 120 h trajectories and then removing the cases affected by fresh pollution. The median and third-quartile radon levels are diminished by almost two-thirds when LCL increases from 10 to 80 h, with a clear drop occurring between 60 and 80 h since the last contact with land. This provides the basis for a 72 h LCL threshold for identifying marine air masses with little or no influence from land.

Although the discrimination between oceanic and land-influenced air masses is imperfect, largely due to the uncertainties in the trajectory calculations, the agreement between the LCL72 and the $\text{radon} < 1000\text{ mBq m}^{-3}$ criteria (during the campaigns for which this parameter was available) suggests that it is reasonable to apply the LCL72 flag to all of the data treated in this study over the global oceans as the first filter against land influences. In subsequent studies on this oceanic ozone dataset, other filters of land influence can be developed and used to meet the requirements of the type of analysis being undertaken. For example, a more stringent criterion ($\text{radon} < 100\text{ mBq m}^{-3}$) was used to select baseline data at the Kennaok/Cape Grim station (Chambers et al., 2018). The data that met the LCL72 criterion covered 161 037 h (77 % of the original dataset). Note that the data with a LCL of less than 72 h are kept in the data file, as they may be useful for other purposes.

2.2 Aircraft data

Table 2 lists the 48 airborne campaigns included in the toar2_oceans_airborne_data_5000m_250203.csv dataset. The land mask mentioned in Sect. 2.1 was used to extract the airborne observations over the oceans. The high-latitude data ($65\text{--}90^\circ\text{N}$ or $90\text{--}60^\circ\text{S}$) were not masked and were used directly. The original merge-type data files from aircraft observations had different time resolutions, from < 10 to 90 s; particularly for old missions, only a coarse time resolution was available. Considering the temporal coverage and taking advantage of the relatively high temporal resolution of the more recent data, a variable temporal resolution in the range of 10–90 s was used. For campaigns where data with a higher temporal resolution (e.g., 1 Hz) were available, e.g., from FAAM measurements, the data were averaged over 10 s. A total of 424 005 and 252 086 data records for the respective altitudes of < 5000 and $< 2000\text{ m}$ are included in the dataset, covering a period from 1987 to 2020. The data originated from the USA, the UK, and Germany/Canada, and they covered almost all global regions except for the R4 region (tropical Indian Ocean). Data for R5 (southern Indian Ocean) were sparse: only 62 points from the TRACE-A mission. The instruments used for the measurements of ozone are generally based on fast-response instruments, e.g., high-sensitivity chemiluminescence or UV absorption. Additional data on observations of pollutant tracers, i.e., CO, NO, and NO_2 , were archived together (Table S2). The backward trajectories were applied to each measurement point, similar to the ship/buoy-based data, with the starting altitude set to the GPS altitude of the aircraft or to 500 m when it was lower. The proportions of the data meeting the LCL72 criterion were 74 % and 63 % for the < 5000 and $< 2000\text{ m}$ cases, respectively. This was partly affected by the assumed top altitude boundary of “land” at 2500 m. The bottom panel of Fig. 1 shows the data meeting the LCL72 criterion at an altitude $< 2000\text{ m}$.

Table 1. List of cruise/buoy data contained in the ship/buoy data file.

Label	Cruise	Platform	Resolution	Year	Data number	Ancillary data	Instrument	Uncertainty	PI (data manager) [working group member worked on the data]	Regions	Literature	Data source
S1	MR12: MR12- 02	<i>Mirai</i>	1 h	2012	733	CO	Thermo, Model 49C	1 %	Yugo Kanaya	R1	Kanaya et al. (2019)	
S2	MR13: MR13- 04, 05, 06, 14-01, 02	<i>Mirai</i>	1 h	2013	2605	CO	Thermo, Model 49C	1 %	Yugo Kanaya	R1, 2, 4, 10	Kanaya et al. (2019)	
S3	MR14: MR14- 04, 05, 06	<i>Mirai</i>	1 h	2014	3561	CO	Thermo, Model 49C	1 %	Yugo Kanaya	R1, 2, 4, 10	Kanaya et al. (2019)	
S4	MR15: MR15- 03, 04, 05	<i>Mirai</i>	1 h	2015	2374	CO	Thermo, Model 49C	1 %	Yugo Kanaya	R1, 2, 5, 10	Kanaya et al. (2019)	
S5	MR16: MR16- 06, 08, 09	<i>Mirai</i>	1 h	2016	2393	CO	Thermo, Model 49C	1 %	Yugo Kanaya	R1, 2, 3, 10, 11	Kanaya et al. (2019)	
S6	MR17: MR17- 05C, 08	<i>Mirai</i>	1 h	2017	2662	CO	Thermo, Model 49C	1 %	Yugo Kanaya	R1, 2, 4, 10		https://doi.org/ 10.17596/0001879 (JAMSTEC, 2017), https://doi.org/10.17596/0001881 (JAMSTEC, 2018a), https://doi.org/10.17596/0001882 (JAMSTEC, 2018b)
S7	MR18: MR18- 04, 05C, 06	<i>Mirai</i>	1 h	2018	2567	CO	Thermo, Model 49C	1 %	Yugo Kanaya	R1, 2, 3, 10, 11		https://doi.org/ 10.17596/0001886 (JAMSTEC, 2018c), https://doi.org/10.17596/0001887 (JAMSTEC, 2018d), https://doi.org/10.17596/0001888 (JAMSTEC, 2018e), https://doi.org/10.17596/0001889 (JAMSTEC, 2018a), https://doi.org/10.17596/0001976 (JAMSTEC, 2019c)
S8	MR19: MR19- 03C, 04	<i>Mirai</i>	1 h	2019	2712	CO	2B Technologies, Model 205	1 %	Yugo Kanaya	R1, 2, 4, 5, 10, 11		https://doi.org/ 10.17596/0002152 (JAMSTEC, 2020b), https://doi.org/10.17596/0002165 (JAMSTEC, 2020c), https://doi.org/10.17596/0002110 (JAMSTEC, 2020d), https://doi.org/10.17596/0002118 (JAMSTEC, 2020e)
S9	MR20: MR20- E01, 05C, E02, 01	<i>Mirai</i>	1 h	2020	2787	CO	2B Technologies, Model 205	1 %	Yugo Kanaya	R1, 2, 10		https://doi.org/ 10.17596/0002152 (JAMSTEC, 2020b), https://doi.org/10.17596/0002165 (JAMSTEC, 2020c), https://doi.org/10.17596/0002110 (JAMSTEC, 2020d), https://doi.org/10.17596/0002121 (JAMSTEC, 2020e)

Table 1. Continued.

Label	Cruise	Platform	Resolution	Year	Data number	Ancillary data	Instrument	Uncertainty	PI (data manager) [working group member worked on the data]	Regions	Literature	Data source
S10	MR21: 05C, 06	<i>Mirai</i>	1 h	2021	2990	CO	2B Technologies, Model 205	1 %	Yugo Kanaya	R1, 2, 10		
S11	KH-18-6	<i>Hakuhō Maru</i>	1 h	2018	527	CO	2B Technologies, Model 205	1 %	Yugo Kanaya	R4, 5	Ueda et al. (2023)	https://doi.org/10.17596/0002308 (JAMSTEC, 2021a), https://doi.org/10.17596/0002310 (JAMSTEC, 2021b), https://doi.org/10.17596/0002331 (JAMSTEC, 2021c), https://doi.org/10.17596/0002312 (JURCAOSS & JAMSTEC, 2021), https://doi.org/10.17596/0002313 (JURCAOSS & JAMSTEC, 2022)
S12	NAAMES1	<i>Atlantis</i>	1 h	2015	525	CN	Thermo, Model 49C	±(2+5 %) ppb	James Johnson	R7		https://www.pmel.noaa.gov/acg/data/ (last access: 6 September 2025)
S13	NAAMES2	<i>Atlantis</i>	1 h	2016	529	CN	Thermo, Model 49C		James Johnson	R7		https://www.pmel.noaa.gov/acg/data/ (last access: 6 September 2025)
S14	NAAMES3	<i>Atlantis</i>	1 h	2017	486	CN	Thermo, Model 49C		James Johnson	R7		https://www.pmel.noaa.gov/acg/data/ (last access: 6 September 2025)
S15	NAAMES4	<i>Atlantis</i>	1 h	2018	497	CN	Thermo, Model 49C		James Johnson	R7, 8		https://www.pmel.noaa.gov/acg/data/ (last access: 6 September 2025)
S16	ATOMIC	<i>Ronald H. Brown</i>	1 h	2020	695	CN	Thermo, Model 49C		James Johnson	R8		https://www.pmel.noaa.gov/acg/data/ (last access: 6 September 2025)
S17	DYNAMO	<i>Roger Revelle</i>	1 h	2011	1130	CN	Thermo, Model 49C		James Johnson	R4, 5		https://www.pmel.noaa.gov/acg/data/ (last access: 6 September 2025)
S18	WACS	<i>Knorr</i>	1 h	2014	192	CN	Thermo, Model 49C		James Johnson	R7		https://www.pmel.noaa.gov/acg/data/ (last access: 6 September 2025)
S19	VOCALS	<i>Ronald H. Brown</i>	1 h	2008	745	CN	TECO49		James Johnson	R2, 3		https://www.pmel.noaa.gov/acg/data/ (last access: 6 September 2025)
S20	MAGE92	<i>John V. Vickers</i>	1 h	1992	670	CN	Dasibi 1008-AH	N/A	James Johnson	R1, 2		https://www.pmel.noaa.gov/acg/data/ (last access: 6 September 2025)
S21	RITS93	<i>Surveyor</i>	1 h	1993	939	CN	Dasibi 1008-AH	N/A	James Johnson	R1, 2, 3, 9, 11		https://www.pmel.noaa.gov/acg/data/ (last access: 6 September 2025)
S22	RITS94	<i>Surveyor</i>	1 h	1994	965	CN	Dasibi 1008-AH and TECO49	N/A	James Johnson	R1, 2, 3, 9, 11		https://www.pmel.noaa.gov/acg/data/ (last access: 6 September 2025)
S23	ACEI	<i>Discoverer</i>	1 h	1995	1102	CN	Dasibi 1008-AH and TECO49	N/A	James Johnson	R1, 2, 3		https://www.pmel.noaa.gov/acg/data/ (last access: 6 September 2025)
S24	ACE-Asia	<i>Ronald H. Brown</i>	1 h	2001	808	CN	Dasibi 1008-AH and TECO49	N/A	James Johnson	R1		https://www.pmel.noaa.gov/acg/data/ (last access: 6 September 2025)

Table 1. Continued.

Label	Cruise	Platform	Resolution	Year	Data number	Ancillary data	Instrument	Uncertainty	PI (data manager) [working group member worked on the data]	Regions	Literature	Data source
S25	NEAQS 2002	Ronald H. Brown	1 h	2002	467	NO, NO ₂	Dasibi 1008-AH and TECO 49	±(2 % + 1 ppb)	(Kenneth Aikin)	R7		https://cs1.noaa.gov/projects/heads/ (last access: 6 September 2025)
S26	NEAQS 2004	Ronald H. Brown	1 h	2004	699	CO, NO, NO ₂	Dasibi 1008-AH and TECO 49	±(2 + 5 %) ppb	(Kenneth Aikin)	R7		https://cs1.noaa.gov/projects/2004/ (last access: 6 September 2025)
S27	TEAQS 2006	Ronald H. Brown	1 h	2006	604	CO, NO, NO ₂	TECO 49c	±(3 % + 0.05) ppbv	(Kenneth Aikin)	R7		https://cs1.noaa.gov/projects/2006/ (last access: 6 September 2025)
S28	ICFALOT	Knorr	1 h	2008	726	CO, NO, NO ₂ , CN	TECO 49c	±(2 % + 0.05) ppbv	Kenneth Aikin and James Johnson	R7, 10		https://cs1.noaa.gov/groups/csl7/ measurements/2008ICFALOT/
S29	CalNex 2010	Atlantis	1 h	2010	473	CO, NO, NO ₂	Thermo Environmental 49c	±(2 % + 1) ppb	(Kenneth Aikin)	R1		https://cs1.noaa.gov/projects/calnex/ (last access: 6 September 2025)
S30	MALASPINA	Hespérée	1 h	2010	3733	NA	UV absorption/2B Technologies, Model 205	NA	Alfonso Saiz-Lopez	R1, 2, 3, 5, 7, 8, 9	Prados-Roman et al. (2015)	
S31	DRAKE2009	Polarstern	1 h	2009	215	NA	UV absorption/2B Technologies	NA	[Theodore Koenig]	R9		https://cs1.seadatanet.org/report/21000666 (last access: 6 September 2025)
S32	MAP-IO/ SWING 2021	Marion Dufresne	1 h	2021	938	NA	HORIBA APOA-370	NA	Aurélie Colomb and Pierre Tulet	R5	Tulet et al. (2024)	http://www.mapio.re/ (last access: 6 September 2025)
S33	MAP IO/OP1 TAAF 2021	Marion Dufresne	1 h	2021	630	NA	HORIBA APOA-370	NA	Aurélie Colomb and Pierre Tulet	R4, 5	Tulet et al. (2024)	http://www.mapio.re/https://www.aeris-data.fr/catalogue-map-io/ (last access: 6 September 2025)
S34	MAP IO/ SCRATCH 2021	Marion Dufresne	1 h	2021	342	NA	HORIBA APOA-370	NA	Aurélie Colomb and Pierre Tulet	R4, 5	Tulet et al. (2024)	http://www.mapio.re/https://www.aeris-data.fr/catalogue-map-io/ (last access: 6 September 2025)
S35	MAP IO/OP2 TAAF 2021	Marion Dufresne	1 h	2021	593	NA	HORIBA APOA-370	NA	Aurélie Colomb and Pierre Tulet	R4, 5	Tulet et al. (2024)	http://www.mapio.re/https://www.aeris-data.fr/catalogue-map-io/ (last access: 6 September 2025)
S36	MAP IO/MAYOBS 2021	Marion Dufresne	1 h	2021	438	NA	HORIBA APOA-370	NA	Aurélie Colomb and Pierre Tulet	R4, 5	Tulet et al. (2024)	http://www.mapio.re/https://www.aeris-data.fr/catalogue-map-io/ (last access: 6 September 2025)
S37	MAP IO/OP3 TAAF 2021	Marion Dufresne	1 h	2021	600	NA	HORIBA APOA-370	NA	Aurélie Colomb and Pierre Tulet	R5	Tulet et al. (2024)	http://www.mapio.re/https://www.aeris-data.fr/catalogue-map-io/ (last access: 6 September 2025)
S38	MAP IO/OP4 TAAF 2021	Marion Dufresne	1 h	2021	549	NA	HORIBA APOA-370	NA	Aurélie Colomb and Pierre Tulet	R4, 5	Tulet et al. (2024)	http://www.mapio.re/https://www.aeris-data.fr/catalogue-map-io/ (last access: 6 September 2025)

Table 1. Continued.

Label	Cruise	Platform	Resolution	Year	Data number	Ancillary data	Instrument	Uncertainty	PI (data manager) [working group member worked on the data]	Regions	Literature	Data source
S39	Ka'iminoma	<i>Ka'iminoma</i>	1 h	2012	505	NA	NA	Rainer Volkamer and Theodore Koenig	R2, 3	Coburn et al. (2014)	https://www.eol.ucar.edu/field_projects/torero (last access: 6 September 2025)	

DWD-MPI
Meteor,
Polarstern,
Walther Herwig,
Anton Dohrn,
Ymer,
Academie
Fedorov,
(DWD);
1977–1996)
+
Berlin Express
(MPI;
1995–2002);
Meteo
(MPI;
2002)

1 h

1977–2002

103 352

NA

1977–1996: a wet chemical instrument using the potassium iodide (KI) method; 1995–2002: Thermo Instrument UV absorption; 2002: Thermo Environmental, 49 and 49c

1977–1996: ±5 ppb; 1995–2002: 6% ± 2 ppb; 2002: < 5%

R3, 5, 7, 8, 9, 10, 11 (2004)

Lebelveld et al. (2004)

Table 1. Continued.

Label	Cruise	Platform	Resolution	Year	Data number	Ancillary data	Instrument	Uncertainty	PI (data manager) [working group member worked on the data]	Regions	Literature	Data source
S41	17v01	<i>Investigator</i>	1 h	2017	1067	N/A	Thermo Scientific, Model 49i analyzer $\times 2$	2.3 %–2.9 %	Suzie Molloy	R3, 11		https://doi.csiro.au/ (last access: 6 September 2025)
S42	17v02	<i>Investigator</i>	1 h	2017	223	N/A	Thermo Scientific, Model 49i $\times 2$		Suzie Molloy	R3		
S43	17v03	<i>Investigator</i>	1 h	2017	729	N/A	Thermo Scientific, Model 49i $\times 2$		Suzie Molloy	R3		
S44	17v04	<i>Investigator</i>	1 h	2017	412	N/A	Thermo Scientific, Model 49i $\times 2$		Suzie Molloy	R3		
S45	17v05	<i>Investigator</i>	1 h	2017	670	N/A	Thermo Scientific, Model 49i $\times 2$		Suzie Molloy	R3		
S46	18v01	<i>Investigator</i>	1 h	2018	864	N/A	Thermo Scientific, Model 49i $\times 2$		Suzie Molloy	R2, 3, 5		
S47	18v02	<i>Investigator</i>	1 h	2018	359	N/A	Thermo Scientific, Model 49i $\times 2$		Suzie Molloy	R3, 11		
S48	18v03	<i>Investigator</i>	1 h	2018	397	N/A	Thermo Scientific, Model 49i $\times 2$		Suzie Molloy	R3		
S49	18v04	<i>Investigator</i>	1 h	2018	588	N/A	Thermo Scientific, Model 49i $\times 2$		Suzie Molloy	R3		
S50	18v05	<i>Investigator</i>	1 h	2018	657	N/A	Thermo Scientific, Model 49i $\times 2$		Suzie Molloy	R3		
S51	18v06	<i>Investigator</i>	1 h	2018	581	N/A	Thermo Scientific, Model 49i $\times 2$		Suzie Molloy	R3		
S52	18v08	<i>Investigator</i>	1 h	2018	284	N/A	Thermo Scientific, Model 49i $\times 2$		Suzie Molloy	R3		
S53	19v01	<i>Investigator</i>	1 h	2019	848	N/A	Thermo Scientific, Model 49i $\times 2$		Suzie Molloy	R3, 11		
S54	19v02	<i>Investigator</i>	1 h	2019	425	N/A	Thermo Scientific, Model 49i $\times 2$		Suzie Molloy	R3		
S55	19v03	<i>Investigator</i>	1 h	2019	667	N/A	Thermo Scientific, Model 49i $\times 2$		Suzie Molloy	R2, 3, 5		

Table 1. Continued.

Label	Cruise	Platform	Resolution	Year	Data number	Ancillary data	Instrument	Uncertainty	PI (data manager) [working group member worked on the data]	Regions	Literature	Data source
S56	IIOE2	<i>Sagar Nidhi</i>	1 h	2015	211	NA	Ecotech EC9810B	1 ppbv	Anoop Mahajan	R4, 5	Mahajan et al. (2019), Inamdar et al. (2020)	
S57	SOE9	S.A. Ag- <i>ulhas</i>	1 h	2016	1121	NA	Ecotech EC9810B	1 ppbv	Anoop Mahajan	R5, 11		
S58	SOE11	S.A. Ag- <i>ulhas</i>	1 h	2020	824	NA	Ecotech EC9810B	1 ppbv	Anoop Mahajan	R5, 11		

Table 1. Continued.

Label	Cruise	Platform	Resolution	Year	Data number	Ancillary data	Instrument	Uncertainty	PI (data manager) [working group member worked on the data]	Regions	Literature	Data source
B1	O-Buoy01	O-Buoy	1 h	2009–2010	4741	NA	Custom-built 2B Technologies, Model 205 dual-beam ozone monitors	Manufacturer-specified limit of detection of 1 ppb; individual measurement uncertainty was calculated to range from 2.1 to 3.5 ppb	John W. Hafacra	R10	Halfacre et al. (2014)	
B2	O-Buoy02	O-Buoy	1 h	2010–2011	2832	NA			John W. Hafacra	R10		
B3	O-Buoy03	O-Buoy	1 h	2010–2011	1405	NA			John W. Hafacra	R10		
B4	O-Buoy04	O-Buoy	1 h	2010–2012	4424	NA			John W. Hafacra	R10		
B5	O-Buoy05	O-Buoy	1 h	2011–2012	1036	NA			John W. Hafacra	R10		
B6	O-Buoy06	O-Buoy	1 h	2012	338	NA			John W. Hafacra	R10		
B7	O-Buoy07	O-Buoy	1 h	2012–2013	955	NA			John W. Hafacra	R10		
B8	O-Buoy08	O-Buoy	1 h	2012–2016	2823	NA			John W. Hafacra	R10		
B9	O-Buoy09	O-Buoy	1 h	2013	46	NA			John W. Hafacra	R10		
B10	O-Buoy10	O-Buoy	1 h	2013–2014	3777	NA			John W. Hafacra	R10		
B11	O-Buoy11	O-Buoy	1 h	2014–2015	3338	NA			John W. Hafacra	R10		
B12	O-Buoy12	O-Buoy	1 h	2014–2015	851	NA			John W. Hafacra	R10		
B13	O-Buoy13	O-Buoy	1 h	2015–2016	1881	NA			John W. Hafacra	R10		
B14	O-Buoy14	O-Buoy	1 h	2015–2017	6229	NA			John W. Hafacra	R10		
B15	O-Buoy15	O-Buoy	1 h	2015–2016	389	NA			John W. Hafacra	R10		
S59	YES-AQ	Gisang I	1 h	2015–2021	2156	NA	Thermo, Model 49C	1 ppb	Junsu Gil	R1	Ahn et al. (2024)	
S60	MOSAiC	Polarstern	1 h	2019–2020	8131	CO	Thermo Fisher Scientific, Model 49i/49C; 2B Technologies, Model 205	Manufacturer-specified precision of 1.0 ppb for 20 s averages, CO 1.5 ppb (5 min)	Julia Schmale	R10	Angot et al. (2022)	https://doi.pangaea.de/10.1594/PANGAEA.944393 (Angot et al., 2022b), https://doi.pangaea.de/10.1594/PANGAEA.944389 (Angot et al., 2022c)

Table 1. Continued.

Label	Cruise	Platform	Resolution	Year	Data number	Ancillary data	Instrument	Uncertainty	PI [data manager] [working group]	Regions	Literature	Data source
S61	SAGA3	Konoe	1 h	1990	562	NA	Dasibi 1008-AH	±3 ppbv	James Johnson	R8	Thompson et al. (1993)	https://saga-pmel.noaa.gov/data/ (last access: 6 September 2025)
S62	AEROSOLS99- INDOEX	Ronald H. Brown	1 h	1999	1392	CN	Dasibi 1008-AH and TECO49	NA	James Johnson	R4, 5, 7, 8, 9		https://www.pmel.noaa.gov/acg/data/ (last access: 6 September 2025)

Note that NA represents “not available”.

2.3 Ozonesonde data

A total of 29 selected ozonesonde launch sites/campaigns are included in the `toar2_oceans_ozonesondedata_250203.csv` dataset. The sites are listed in Table S3 and shown in Fig. 1. There are no data for regions R4 (Indian Ocean) and R9 (South Atlantic). As the availability of geopotential height information was considered a high priority in the creation of the dataset, data from earlier dates when this parameter was not available (e.g., Alert before 2000) were not included. Their inclusion could be a future task. The ozone mixing ratio was calculated from the atmospheric pressure and the ozone partial pressure data. To reduce the data volume, one data point every 200 m (data closest to the top of each layer, e.g., near 200 or 400 m) was extracted up to a 5000 m altitude. The ($1/e$) ozone sensor response time (~ 30 s) gives the ozonesonde a vertical resolution of about 150 m for a typical balloon ascent rate (Van Malderen et al., 2025). Most of the sites (24 out of 29) were taken from the homogenized HEGIFTOM dataset (Van Malderen et al., 2025) to ensure data quality. The selected launch sites are on islands or close to the coast. The other five data sources are from island and shipboard campaigns in the tropical Pacific (Gómez Martín et al., 2016; Shiotani et al., 2002; Fujiwara et al., 2003), with the addition of three datasets in R11 (Antarctic region) from the World Ozone and Ultraviolet Radiation Data Centre (WOUDC) ozonesonde database to improve the coverage. The data are all from electrochemical concentration cell (ECC)-type ozonesondes. In total, 666 470 and 254 276 data points below respective altitudes of 5000 and 2000 m were collected.

Backward-trajectory calculations were only performed for selected heights (500, 1000, 1500, 2000, 3000, 4000, and 5000 m) to reduce the computational cost. The LCL information relative to the closest of the height points was used. The proportions of the data meeting the LCL72 criterion were 80 % and 67 % for the full dataset (< 5000 m altitude) and for the < 2000 m data subset, respectively. As the launch site is usually on land, the latitude/longitude information from the backward trajectories at 0 and 1 h prior to launch was not included in the LCL calculation. Therefore, the potential influence of local air pollution in the vicinity of the launch site needs to be considered when using these data. For a further characterization of air masses and screening, wind direction sector information (Table S3), constructed from the coordinates from the backward-trajectory files at 0 and 1 h before launch, was added to the dataset.

2.4 Non-polar coastal site data

The list of 21 non-polar coastal sites included in the `toar2_oceans_coastsites_250203.csv` file is shown in Table S4, and their locations are given in Fig. 1: 16 sites are from the TOAR-II database (Schröder et al., 2024), 2 are from field campaigns, 2 are from the EANET monitoring net-

Table 2. List of aircraft-based campaign data contained in the aircraft dataset.

Label	Campaign	Platform	Resolution	Year	Data number < 5000 m < 2000 m	Ancillary data	Instrument	Uncertainty	PI (data manager) [working group member worked on the data]	Regions	Literature	Data source	
A1	ABLE-2B	Electra	60 s	1987	67	677	CO	NA	(Gao Chen)	R7, 8	Harris et al. (1990)	https://www.gie.larc.nasa.gov/gie_mrg1.htm#ABLE-2B (last access: 6 September 2025)	
A2	ABLE-3A	Electra	60 s	1988	1668	3824	NO	NA	2 ppbv (detection limit)	(Gao Chen)	R1, 7, 10	Harris et al. (1992)	https://www.gie.larc.nasa.gov/gie_mrg1.htm#ABLE-3A (last access: 6 September 2025)
A3	ABLE-3B	Electra	90 s	1990	133	258	CO, NO, NO ₂	NA	(Gao Chen)	R7, 10	Harris et al. (1994)	https://www.gie.larc.nasa.gov/gie_mrg1.htm#ABLE-3B (last access: 6 September 2025)	
A4	CITE-3	Electra	10 s	1989	21 355	28 718	CO	Chemiluminescence	N/A	(Gao Chen)	R7, 8	Hoell et al. (1993)	https://www.gie.larc.nasa.gov/gie_mrg1.htm#CITE-3 (last access: 6 September 2025)
A5	PEM-West A	DC-8	90 s	1991	801	1511	CO, NO, NO ₂	Chemiluminescence	5 % or 2 ppb	(Gao Chen)	R1, 2	Hoell et al. (1996)	https://www.gie.larc.nasa.gov/gie_mrg1.htm#PMWEST-A (last access: 6 September 2025)
A6	PEM-West B	DC-8	30 s	1994	2142	5259	CO, NO	Chemiluminescence	3 % or 2 ppb	(Gao Chen)	R1, 2	Hoell et al. (1997)	https://www.gie.larc.nasa.gov/gie_mrg1.htm#PMWEST-B (last access: 6 September 2025)
A7	TRACE-A	DC-8	90 s	1992	131	408	CO, NO, NO ₂	NA	(Gao Chen)	R5, 7, 8, 9	Fishman et al. (1996)	https://www.gie.larc.nasa.gov/gie_mrg1.htm#TRACE-A (last access: 6 September 2025)	
A8	PEM-Tropics A	DC-8	60 s	1996	1395	2969	CO, NO, NO ₂	Chemiluminescence	3 % or 2 ppb	(Gao Chen)	R1, 2, 3, 11	Hoell et al. (1999)	https://www.gie.larc.nasa.gov/gie_mrg1.htm#PTROPICS-A (last access: 6 September 2025)
A9	PEM-Tropics B P3B	P3B	60 s	1999	3111	4939	CO, NO, NO ₂	Chemiluminescence	3 % or 2 ppb	(Gao Chen)	R1, 2, 3, 7	Raper et al. (2001)	https://www.gie.larc.nasa.gov/gie_mrg1.htm#PTROPICS-B (last access: 6 September 2025)
A10	PEM-Tropics B DC8	DC-8	60 s	1999	1573	3027	CO, NO, NO ₂	Chemiluminescence	3 % or 2 ppb	(Gao Chen)	R1, 2, 3, 8	Hoell et al. (1999)	https://www.gie.larc.nasa.gov/gie_mrg1.htm#PTROPICS-B (last access: 6 September 2025)
A11	TRACE-P P3B	P3B	60 s	2001	3036	6374	CO, NO, NO ₂	Chemiluminescence	5 % or 2 ppb	(Gao Chen)	R1, 2, 7	Jacob et al. (2003)	https://www.gie.larc.nasa.gov/gie_mrg1.htm#TRACE-P (last access: 6 September 2025)
A12	TRACE-P DC8	DC-8	60 s	2001	2024	3925	CO, NO, NO ₂	Chemiluminescence	5 % or 2 ppb	(Gao Chen)	R1, 2	Singh et al. (2006)	https://www.gie.larc.nasa.gov/gie_mrg1.htm#TRACE-P (last access: 6 September 2025)
A13	INTEX-NA	DC-8	60 s	2004	1056	1739	CO, NO, NO ₂	Chemiluminescence	5 % or 1 ppb	(Gao Chen)	R1, 7		https://www.gie.larc.nasa.gov/gie_mrg1.htm#INTEX-NA (last access: 6 September 2025)
A14	INTEX-B DC8	DC-8	60 s	2006	1262	2695	CO, NO, NO ₂	Chemiluminescence	1 ppb or 5 %	(Gao Chen)	R1, 2, 7	Singh et al. (2009)	https://www.gie.larc.nasa.gov/gie_mrg1.htm#INTEX-B (last access: 6 September 2025)
A15	INTEX-B C-130	C-130	60 s	2006	741	2468	CO, NO, NO ₂	Chemiluminescence	0.1 ppbv or 5 %	(Gao Chen)	R1, 2, 7	Shon et al. (2008), Kleib et al. (2011)	https://www.gie.larc.nasa.gov/gie_mrg1.htm#INTEX-B (last access: 6 September 2025)
A16	ARCTAS	DC-8	60 s	2008	1287	2444	CO, NO, NO ₂	Chemiluminescence	±2 ppbv	Andrew Weinheimer, Denise Montzka, David Knapp, and Ilana Pollack	R1, 10	Jacob et al. (2010)	https://www.gie.larc.nasa.gov/gie_mrg1.htm#ARCTAS (last access: 6 September 2025)
A17	SEAC4RS DC8	DC-8	60 s	2013	376	601	CO, NO, NO ₂	Chemiluminescence	0.030 ppbv + 3 %	Tom Ryerson, Jeff Peischl, and Ileana Pollack	R1, 7		https://www.gie.larc.nasa.gov/gie_mrg1.htm#SEAC4RS (last access: 6 September 2025)
A18	SEAC4RS ER2	ER2	60 s	2013	83	202	CO	UV absorption	3 % ± precision	(Gao Chen)	R7		https://www.gie.larc.nasa.gov/gie_mrg1.htm#SEAC4RS (last access: 6 September 2025)
A19	DISCOVER-AQ	P3B	60 s	2013	145	162	NO, NO ₂	Four-channel chemiluminescence	0.1 ppbv + 5 %	(Gao Chen)	R1		https://www.gie.larc.nasa.gov/gie_mrg1.htm#DISCOVER-AQ (last access: 6 September 2025)
A20	KORUS-AQ	DC-8	60 s	2016	2057	2631	CO, NO, NO ₂	Four-channel chemiluminescence,	5 ppbv + 10 %	(Gao Chen)	R1		https://www.gie.larc.nasa.gov/gie_mrg1.htm#KORUS-AQ (last access: 6 September 2025)

Table 2. Continued.

Label	Campaign	Platform	Resolution	Year	Data number < 2000 m	Data number <500 m	Ancillary data	Instrument	Uncertainty	PI (data manager) (working group member worked on the data)	Regions	Literature	Data source
A21	ATom1-4	DC-8	10 s	2016–2018	23715	42975	CO, NO, NO ₂	Four-channel chemiluminescence	5–10 ppt	Iann Bougeouis, Jeff Peischl, and J. Ryan Spackman	R1, 2, 3, 7, 8, 9, 10, 11	Wofsy et al. (2021)	https://doi.org/10.5194/essd-17-4901-2025
A22	HIPPO	NSF NCAR G-V	10 s	2009–2011	20 509	45 018	CO	Ultraviolet absorption	Final data: accuracy approximately ±5 %	David Fahey, Ru-Shan Guo, and J. Ryan Spackman	R1, 2, 3, 7, 8, 10, 11	Bougeouis et al. (2020), Wofsy et al. (2017)	https://www.col.ucar.ac.at/field_projects/hippo (last access: 6 September 2025)
A23	ACCSIS FAAM	FAAM/BaC 146–301	10 s	2017–2020	23 046	34 840	CO	TECO 49	N/A	James Lee	R7, 8	https://catalogue.ceda.ac.uk/uuid/8012e810bc2c49983aa8781bb5fc54d (last access: 6 September 2025); https://www.tiam.ac.uk/sphinx/creditatdynamc_content/modules.html#elczone (last access: 6 September 2025)	
A24	ACCACIA FAAM	FAAM/BaC 146–301	10 s	2013	7 548	11 369	CO			James Lee	R10		
A25	CAST FAAM	FAAM/BaC 146–301	10 s	2014	7210	10 566	CO			James Lee	R1		
A26	CLARIFY FAAM	FAAM/BaC 146–301	10 s	2017	14 248	24 319	CO			James Lee	R8		
A27	ITOP FAAM	FAAM/BaC 146–301	10 s	2004	4683	13 350	CO			James Lee	R7		
A28	VOCALS FAAM	FAAM/BaC 146–301	10 s	2008	19 037	19 756	CO			James Lee	R2, 3		
A29	NARE1996	NOAA P-3	10 s	1996	3 006	4783	CO, NO, NO ₂	NA	NA	Kenneth Aikin	R7		
A30	NARE1997	NOAA P-3	10 s	1997	4 886	9931	CO, NO, NO ₂	NA	NA	Kenneth Aikin	R7		
A31	TEXAQS2000	NCAR Electra	10 s	2000	2 496	3 904	CO, NO, NO ₂	Chemiluminescence	NA	Kenneth Aikin	R7	Ryerson et al. (1998)	https://cds1.noaa.gov/projects/txaqsp2k/ (last access: 6 September 2025)
A32	ITCT2002	NOAA WP-3D	10 s	2002	6 004	13 772	CO, NO, NO ₂	Chemiluminescence	±2 %	Kenneth Aikin	R1, 7		https://cds1.noaa.gov/projects/itct2k2/ (last access: 6 September 2025)
A33	ITCT2004	NOAA WP-3D	10 s	2004	15 213	19 791	CO, NO, NO ₂	Chemiluminescence	0.1 + 3 %)	Kenneth Aikin	R7		https://cds1.noaa.gov/projects/2004/ (last access: 6 September 2025)
A34	HURRICANE2006	NOAA G-4	10 s	2006	3 34	663	none	NA		Kenneth Aikin	R7, 8		https://cds1.noaa.gov/groups/csl7/ measurements/2006/hurricane/ (last access: 6 September 2025)
A35	TEXAQS2006	NOAA WP-3D	10 s	2006	5 395	6 772	CO, NO, NO ₂	Chemiluminescence	0.050 ppbv + 3 %	Kenneth Aikin	R7		https://cds1.noaa.gov/projects/2006/ (last access: 6 September 2025)
A36	ARCPAC2008	NOAA WP-3D	10 s	2008	4 878	11 563	CO, NO, NO ₂	Chemiluminescence	0.05 + 4 %	Kenneth Aikin	R10		https://cds1.noaa.gov/projects/arcpac/ (last access: 6 September 2025)
A37	CalNeX2010	NOAA WP-3D	10 s	2010	7 040	9 265	CO, NO, NO ₂	Chemiluminescence	0.015 ppbv + 2 %	Kenneth Aikin	R1, 7	Pollack et al. (2010)	https://cds1.noaa.gov/projects/calnex/ (last access: 6 September 2025)
A38	WINTERSTORMS2001	NA	10 s	2001	1 64	895	none	NA	NA	Kenneth Aikin	R1		
A39	WINTERSTORMS2002	NA	10 s	2002	8 15	1867	none	NA	NA	Kenneth Aikin	R1, 7		

Table 2. Continued.

Label	Campaign	Platform	Resolution	Year	Data number < 2000 m	Ancillary data	Instrument	Uncertainty	PI (data manager) [working group member worked on the data]	Regions	Literature	Data source
A40	WINTERSTORMS2003	NOAA G-4	10 s	2003	657	2225	none	NA	(Kenneth Aikin)	R1, 7		https://esrl.noaa.gov/groups/cst7/ measurements/2003WinterStorms/ (last access: 6 September 2025)
A41	WINTERSTORMS2004	NOAA G-4	10 s	2004	992	3283	none	NA	(Kenneth Aikin)	R1, 2, 7		https://esrl.noaa.gov/groups/cst7/ measurements/2004WinterStorms/ (last access: 6 September 2025)
A42	WINTERSTORMS2005	NOAA G-4	10 s	2005	541	2099	none	NA	(Kenneth Aikin)	R1		https://esrl.noaa.gov/groups/cst7/ measurements/2005WinterStorms/ (last access: 6 September 2025)
A43	WINTERSTORMS2006	NOAA G-4	10 s	2006	900	1633	none	NA	(Kenneth Aikin)	R1		https://esrl.noaa.gov/groups/cst7/ measurements/2006WinterStorms/ (last access: 6 September 2025)
A44	WINTERSTORMS2007	NOAA G-4	10 s	2007	355	1375	none	NA	(Kenneth Aikin)	R1, 7		https://esrl.noaa.gov/groups/cst7/ measurements/2007WinterStorms/ (last access: 6 September 2025)
A45	ACTIVATE	Falcon	60 s	2020	5983	6797	CO	UV absorption greater of ±5 ppbv or ±5 %	(Gao Chen)	R7		<a href="https://www-air.larc.nasa.gov/cgi-bin/
ArcView/activate.2022?HU25=1">https://www-air.larc.nasa.gov/cgi-bin/ ArcView/activate.2022?HU25=1 (last access: 6 September 2025)
A46	CONTRAST	NSF NCAR G-V	10 s	2014	3308	6318	CO, NO, NO ₂ Chemiluminescence	NA	Rainer Volkamer	R1, 2	Pan et al. (2017)	https://www.ec.gc.ca/field_projects/contrast/ (last access: 6 September 2025) https://doi.org/10.3065/DGP/K016N (Weinheimer, 2015)
A47	TORERO	NSF NCAR G-V	10 s	2012	7129	12569	CO	Dual-channel UV absorption spectrometer	Rainer Volkamer	R2, 3, 8	Volkamer et al. (2015)	<a href="https://open.canada.ca/data/en/dataset/
1143472d-6c73-4b5c-bc2b-a3d5319961e9">https://open.canada.ca/data/en/dataset/ 1143472d-6c73-4b5c-bc2b-a3d5319961e9 (last access: 6 September 2025) <a href="https://open.canada.ca/data/en/dataset/
ef0e41c-890d-404d-bb1b-421456022451">https://open.canada.ca/data/en/dataset/ ef0e41c-890d-404d-bb1b-421456022451 (last access: 6 September 2025)
A48	NETCARE	Polar 6	10 s	2014–2015	17551	27496	none	Thermo Scientific, Model 49i	Ralf Staehler	R10	Abbatt et al. (2019)	

Note that NA represents “not available”.

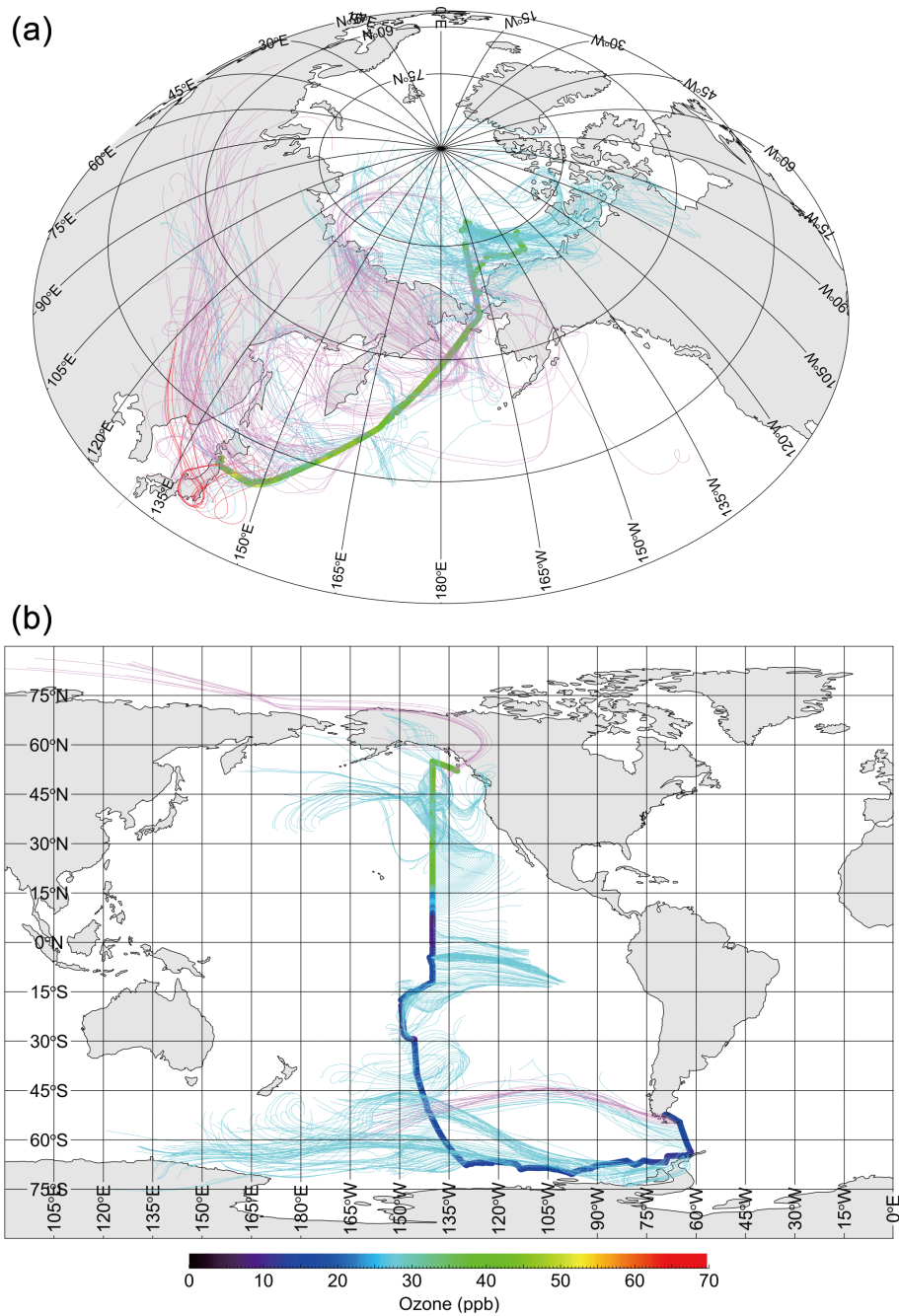


Figure 2. Backward trajectories (120 h long) for observations with oceanic (light blue) and apparently land-influenced (purple) conditions, as assessed with the LCL72 criterion during (a) the MR19-03C observations from 29 September to 10 November 2019 and (b) the RITS94 observations from 23 November 1993 to 6 January 1994. The red lines indicate cases in which the observed ozone mixing ratio is greater than 50 ppb.

work, and 1 is from CSIRO. The sites were selected on the basis of the availability of high-quality data over long periods (typically > 10 years) and for the global coverage. However, no sites matching these criteria could be found for regions R4 and R5 (Indian Ocean). The Kennaook/Cape Grim dataset available on the TOAR-II database was not used; rather, an-

other dataset provided by CSIRO was employed. The latter was an updated version, extended through to the end of 2020, with the years 1982–2017 inclusive being fully QA/QC data on the WMO GAW/BiPM scale. The 2018–2020 period was in the final stages of QA/QC, and the fully finalized dataset has subsequently been published on EBAS (EBAS, 2025).

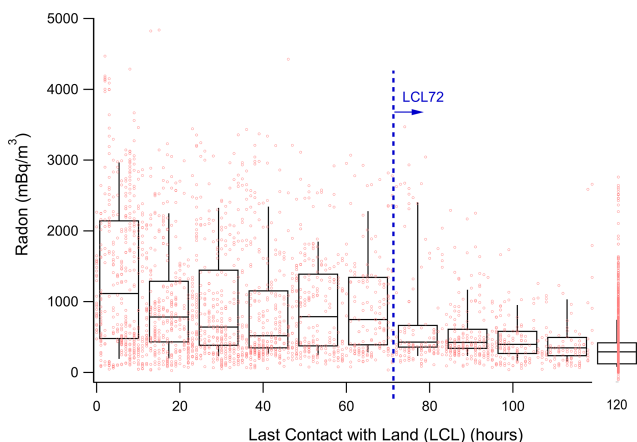


Figure 3. Decrease in radon concentrations with last contact with land from backward-trajectory analysis. ACE-1, ACE-Asia, ATOMIC, ICEALOT, NAAMES1-4, and WACS data were used in combination. Radon data were from NOAA PMEL. The dotted blue line indicates the adopted LCL72 criterion. Boxes and whiskers represent the 10th, 25th, 50th, 75th, and 90th percentiles.

Further information on the instruments and uncertainties for each site can be found in the TOAR-II database. Obviously, the incorrect data (i.e., zero or negative values) have been removed, resulting in a total of 3 650 267 hourly observations being included. The LCL information based on the backward trajectories is included. To reduce the computational cost, only 6 hourly calculations were performed, and the result at the closest data timestamp was used. It should be noted that the risk of the influence from local air pollution is similar to that of the ozonesonde dataset. Data from Trinidad Head can be screened using the local wind direction information (as shown in Table S3).

2.5 Polar site data

The list of 17 polar coastal sites included in the toar2_oceans_polarsites_250203.csv file is shown in Table S5 and Fig. 1. Except for Alert and Belgrano stations, where the data came from the Canadian data site and from the National Institute for Aerospace Technology (INTA), respectively, the 15 datasets are from the TOAR-II database. A total of 3 362 716 hourly observations were included. Similarly to the case of the non-polar coastal sites, the LCL information based on the backward trajectories is included. To save computational cost, only 6-hourly trajectory calculations were performed, and the result at the closest data timestamp was used.

3 Data overview

In this section, some basic data analysis and descriptive statistics of the collected datasets are described, for informational purposes. Detailed discussion of the spatiotempo-

ral distribution of tropospheric ozone and its trends over the oceans and polar regions will be presented in the assessment paper (Sommariva et al., 2025).

3.1 Latitudinal, longitudinal, and vertical transects

Figure 4 shows the latitudinal and longitudinal cross sections of the ship/buoy data after application of the LCL72 filter. The data are grouped into 10° latitudinal and 20° longitudinal bins. The median values in the Southern Hemisphere are in the range of 15.2–19.1 ppb, while those in the Northern Hemisphere are in the range of 20.5–34.0 ppb. As expected, a maximum median value was found between 25 and 55° N, where the ozone is photochemically produced from precursors anthropogenically emitted over the continents and transported over long distances to the open oceans (Fig. 1; see also Kanaya et al., 2019). The longitudinal distribution has less variability, with median values in a narrow range of ca. 20–30 ppb. The high episodes (higher than the 75th percentile) are evident from 35 to 45° N and from 120 to 140° E, suggesting that the effects of Asian pollution remain in the dataset, consistent with the discussion regarding the LCL72 filter.

Figure 5 shows the vertical profiles of the combined aircraft and ozonesonde data after application of the LCL72 filter. The data are grouped into 250 m altitude bins. The general tendency is that ozone mixing ratios increase with height, except in R7 (northern Atlantic), where the minimum median values occur in the 700–950 m layer, and in R8 (Tropical Atlantic), where ozone mixing ratios remain nearly constant from 1950 to 5000 m.

3.2 Seasonal coverage

Table S6 summarizes the number of observation days per region and season. For the ship/buoy dataset, the four seasons were relatively well sampled, but the frequencies were higher for boreal or austral summer than winter for mid- and high-latitude regions (R1, 3, 7, 9, 10, and 11). For the airborne data, coverage was less in summer than in winter over the Pacific, while the opposite was true for the Atlantic. The ozonesonde dataset appeared to have relatively uniform seasonal coverage, except that frequent observations were made during September–October–November over the Antarctic (R11).

3.3 Ship/buoy-based median concentrations and diurnal variation patterns in individual regions (R1–R11)

Table 3 summarizes statistics of hourly data from the ship/buoy dataset (satisfying LCL72) to compare median concentrations across defined regions (R1–R11) and to investigate features of the average diurnal profile (Fig. 6). First, the number of hourly data for individual regions ranged from 3446 (R4) to 61 708 (R10), highlighting the advantage of having this large dataset in one place. For R10 (Arc-

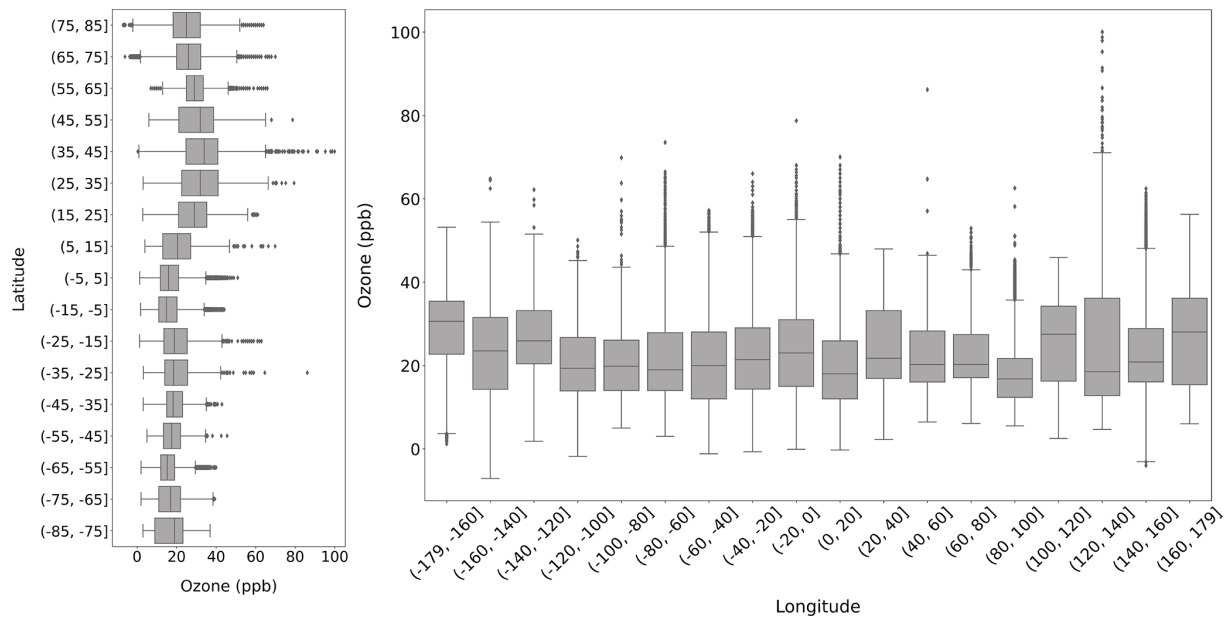


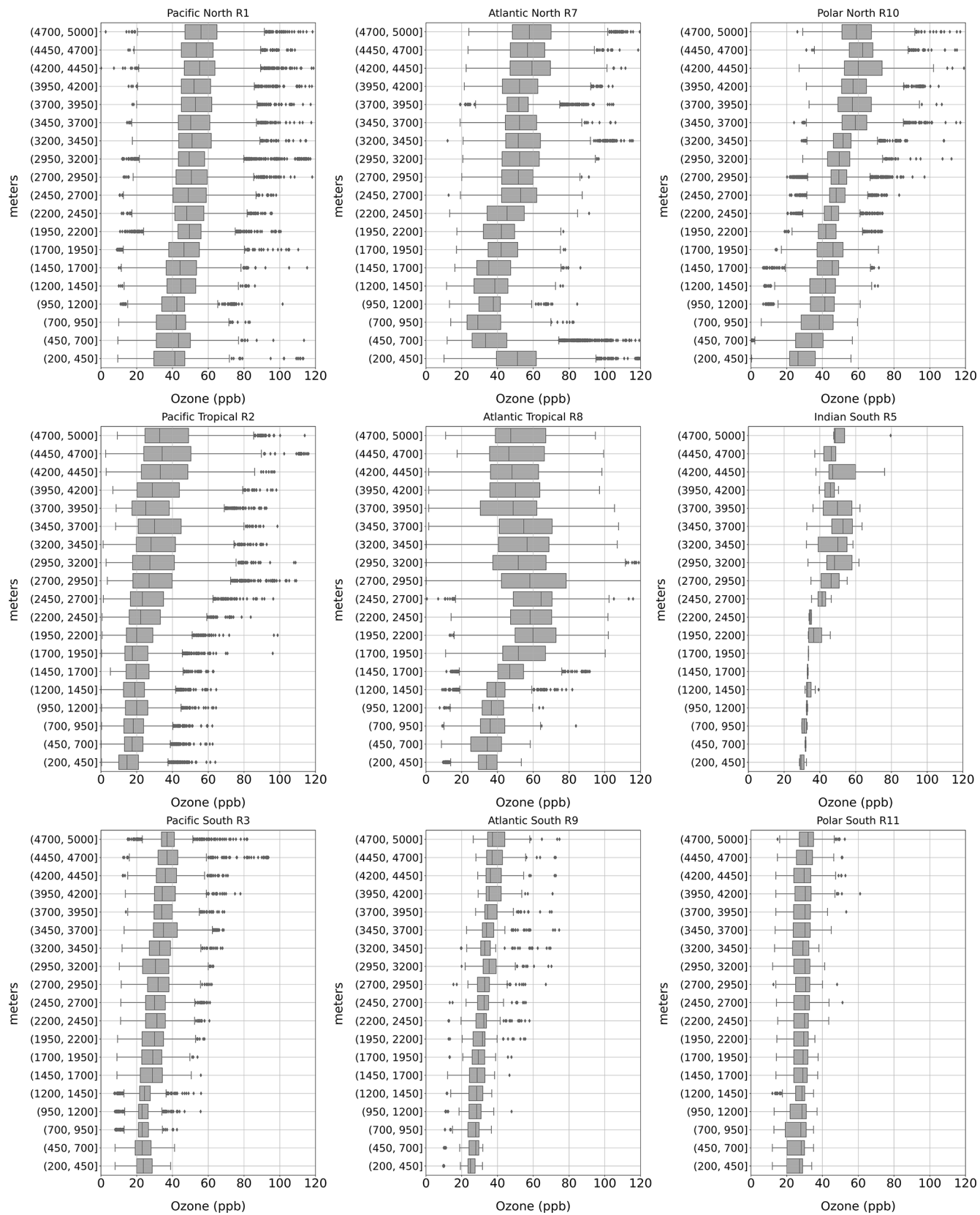
Figure 4. Latitudinal and longitudinal transect of the ship/buoy datasets after filtering for $LCL \geq 72$ h.

tic), 31 549 and 7732 h of data were from the O-Buoy (autonomous, ice-tethered buoy) and MOSAiC (Multidisciplinary drifting Observatory for the Study of Arctic Climate) missions. The datasets for regions R7–R9 (Atlantic), with contributions from the DWD-MPI cruises, were larger than those for the Pacific (R1–R3). For all regions, the data are almost equally distributed over the time of day. The average diurnal profiles were calculated as follows: local time was derived for each point by adjusting the coordinated universal time (UTC) based on longitude; then, the 25th, 50th, and 75th percentiles were calculated for each hourly bin per region.

The average of the hourly medians showed variability across regions. For the northern midlatitudes, the Pacific and Atlantic were similar (32.9 and 31.6 ppb for R1 and R7, respectively). For the tropics, the Pacific (13.8 ppb, R2) was lower than the Indian Ocean (16.2 ppb, R4) and the Atlantic (20.0 ppb, R8). For the southern midlatitudes, the values for the Pacific and Indian oceans were similar (20.1 and 19.7 ppb for R3 and R5, respectively), while the Atlantic was the lowest (15.4 ppb for R9). The R9 value is even lower than that of R8 and close to that of R11 (15.9 ppb, Antarctic). R10 (26.2 ppb) was slightly lower than R1 and R7 (northern midlatitudes). While the mixing ratios over the tropics are frequently below 15 ppb (for 30 %, 50 %, and 59 % of the observations over the Atlantic (R8), Indian (R4), and Pacific (R2) oceans, respectively), they are very rarely near zero (< 1 % of observations are less than 3 ppb; Fig. 7). This is in marked contrast to the Arctic (R10), where a secondary distribution peak is found at around zero, greater mean and median ozone levels are observed, and only 18 % of mixing ratios are less than 15 ppb. Roughly one-third of these are

ozone depletion events (ODEs) and 5.9 % of total observations are below 3 ppb. This indicates that the mechanism(s) of Arctic ODEs is either inoperative or less efficient in the tropics.

As noted in Sect. 1, a unique feature of ozone in the marine boundary layer over the remote oceans is net photochemical loss. This must result in afternoon decreases in ozone levels. Indeed, flat diurnal patterns or daytime decreases are evident for the ship/buoy data in most regions (Fig. 6, Table 3). The diurnal profiles of the oceanic data suggest that the datasets collected are representative of the marine atmosphere. More specifically, the three tropical regions, R2, R4, and R8, show relatively large daytime decreases. The local time at which the minima were recorded was 15, 16, and 15 h for R2, R4, and R8, respectively (Table 3), while the maxima were recorded at night or in the morning. The different timings must be affected by dynamics and chemistry. The amplitude (maximum minus minimum) of the diurnal variation was 1.7, 2.6, and 2.3 ppb or 12 %, 16 %, and 11 % of the mean concentration for R2, R4, and R8, respectively. Previous studies from ship observations (Johnson et al., 1990; Thompson et al., 1993; Dickerson et al., 1999; Watanabe et al., 2005) and from coastal site observations (Oltmans, 1981; Nagao et al., 1999; Galbally et al., 2000; Read et al., 2008; Hu et al., 2010) have focused on diurnal variation with daytime decreases and reported amplitudes of 1–7.5 ppb (7 %–32 % of average concentration levels). These studies are mainly from single sites/campaigns for short periods of time. Our dataset will be useful to investigate the characteristics of ozone diurnal variations more comprehensively and with statistical robustness. Contributions from various chemical pathways (e.g., HO_x and halogen cycles) will be

**Figure 5.** Vertical profiles of ozone concentrations by region after filtering for LCL72.

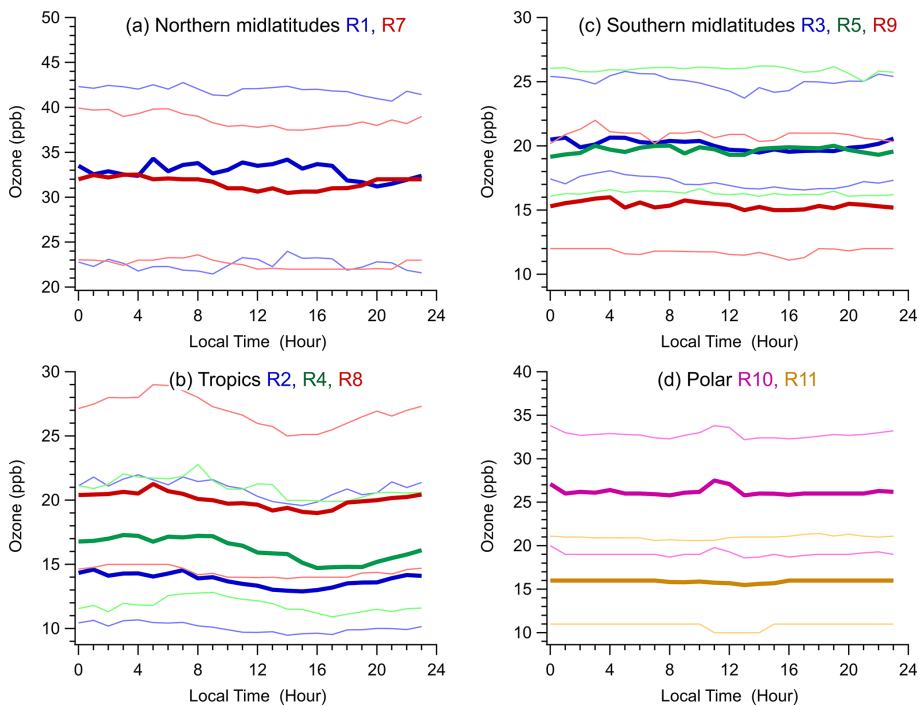


Figure 6. Hourly median (thick lines) and interquartile levels (thin lines) and their diurnal variation by region: (a) R1 and R7 (Pacific and Atlantic northern midlatitudes); (b) R2, R4, and R8 (Pacific, Indian, and Atlantic low latitudes); (c) R3, R5, and R9 (Pacific, Indian, and Atlantic southern midlatitudes); and (d) R10 and R11 (polar, i.e., Arctic and Antarctic regions). The blue, green, and red line colors correspond to the Pacific, Indian, and Atlantic oceans, respectively.

Table 3. Statistics of hourly data from the ship/buoy dataset per defined region (R1–R11).

Regions	Number of hourly data (satisfying LCL72)	Maximum of hourly medians (ppb)	Local time (hour) of maximum	Minimum of hourly medians (ppb)	Local time (hour) of minimum	Average of 24 hourly medians (ppb)	Amplitude (max–min) (ppb)	Percentage amplitude (max–min)/average (%)
R1	6572	34.3	5	31.2	20	32.9	3.1	9.4
R2	9708	14.6	1	12.9	15	13.8	1.7	12.3
R3	6432	20.7	1, 4	19.5	14	20.1	1.2	5.7
R4	3446	17.3	3	14.7	16	16.2	2.6	16.0
R5	5651	20.0	8	19.2	0	19.7	0.9	4.4
R7	14 777	32.5	1, 3, 4	30.5	14	31.6	2.0	6.5
R8	18 818	21.3	5	19.0	15	20.0	2.3	11.3
R9	13 710	16.0	4	15.0	15, 16	15.4	1.0	6.5
R10	61 708	27.5	11	25.8	8, 13	26.2	1.7	6.5
R11	20 215	16.0	0–7, 16–23	15.5	13	15.9	0.5	3.3

discussed by comparison with model simulations in the upcoming assessment paper. We also plan an in-depth analysis of our first observational findings, including the substantial reduction in the tropical Indian Ocean (R4), consistent with Dickerson et al. (1999), and the relatively early onset of daytime destruction for R8 and R2.

3.4 Consistency between the ground-based observations and the ozonesonde observations at the same sites

At six stations (Alert, Ny Ålesund, Trinidad Head, American Samoa, Syowa, and South Pole), both ground-based and ozonesonde observations were recorded. The consistency between the two datasets was checked by comparing ozone measurements at ground level and the ozonesonde

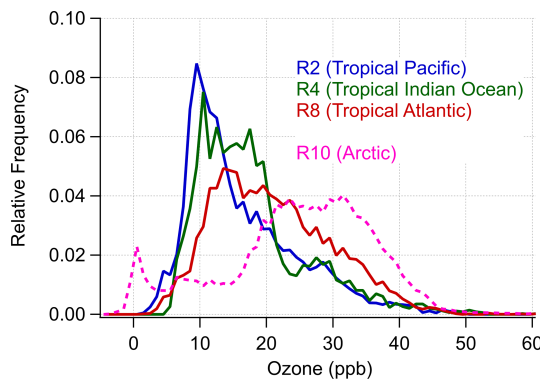


Figure 7. Frequency of observed ozone concentrations in 1 ppb bins computed for ship and buoy observations with LCL ≥ 72 h for tropical regions (Pacific Ocean, R2; Indian Ocean, R4; and Atlantic Ocean, R8) contrasted with the Arctic (R10).

data at the lowest altitude (typically around 200 m). Figure 8 shows 3-year and 2-year comparisons at Alert and American Samoa, as an example. The agreement was found for cases of episodic ozone decreases in the Arctic and for temporal patterns of variation over days and seasons at both sites, demonstrating the internal consistency of the datasets. Using the ground-based and ozonesonde observations in the Arctic (including Alert) for the year of 2015 as well as ship/buoy/aircraft observations, Gong et al. (2025) discuss the performance of two chemistry transport models. Reasonable agreement was also found with scatterplots for all six sites (Fig. S2), with R^2 values ranging from 0.64 to 0.95 and slopes of bivariate linear fits ranging from 0.94 to 1.11 when sonde values were plotted against surface observations made within 1 h of each other. This analysis indicated the high quality of the two datasets.

4 Data availability

The datasets described in this paper are available as five .csv files containing all of the corresponding metadata information. The files are named as follows:

1. toar2_oceans_ship_buoy_data_250203.csv;
2. toar2_oceans_airborne_data_5000m_250203.csv;
3. toar2_oceans_ozonesondedata_250203.csv;
4. toar2_oceans_coastsites_250203.csv;
5. toar2_oceans_polarsites_250203.csv.

The files contain the key metadata information listed in Tables 1–5 and are available at <https://doi.org/10.17596/0004044> (Kanaya et al., 2025).

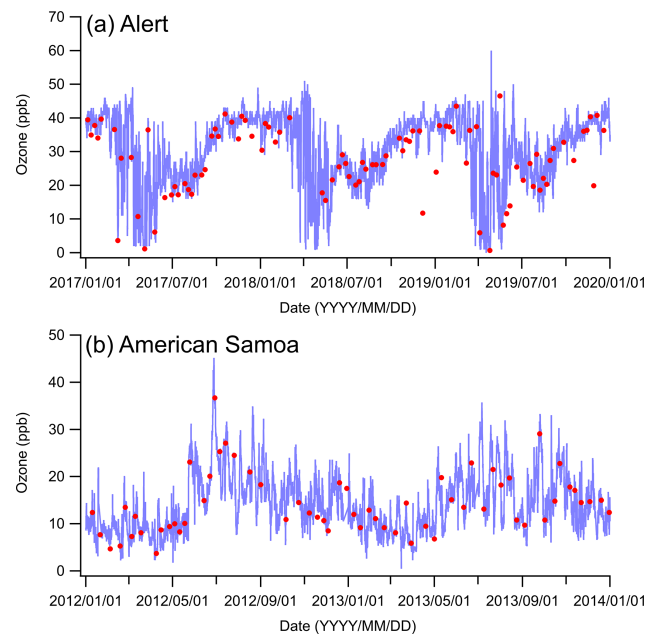


Figure 8. Ozone concentrations from surface observations (blue) and the lowest layer of ozonesonde observations (red, ~ 200 m altitude) at (a) Alert and (b) American Samoa.

5 Conclusions and outlook

Under the TOAR-II activity, the Oceans working group has, for the first time, collected and collated observational ozone data over the open oceans and polar regions on a global scale. When available, additional pollution tracers (CO, NO, NO₂, and CN) were also included. All of these datasets are stored in five data files classified by platform type, i.e., ship/buoy, aircraft, ozonesondes, non-polar coastal sites, and polar sites. Here, we describe the datasets and the details of the preprocessing, filtering, and flagging procedures as well as showing basic analyses of the spatiotemporal extent, diurnal variation characteristics, and internal consistency. Our focus was on the ship/buoy and aircraft observations, which contain a total of 208 291 and 424 005 records, respectively. The aircraft and ozonesonde data covered an altitude range from the surface to 5000 m, allowing a complete assessment of ozone over the oceans and polar regions with a focus on the atmospheric boundary layer (< 2000 m). All datasets were supplemented with information on the number of hours that each observed air mass was separated from land, derived from backward trajectories. The selected criterion of 72 h or more isolation from land, justified by the coincident radon observations for some selected datasets, allowed the identification of marine air masses. Flat diurnal patterns or diurnal decreases were found after air mass selection, indicating that the collected datasets are representative of the marine atmosphere. Over the tropics, the amplitude of the observed daytime decreases was 11 %–16 %, with the largest decrease observed in the Indian Ocean.

Although the observational data have been collected as widely as possible, they are still not sufficiently dense or homogeneous across the defined regions, particularly for the purpose of small trend detection (Chang et al., 2024). In order to interpret the data, the sampling bias needs to be assessed using atmospheric chemistry transport numerical model simulations (e.g., Sekiya et al., 2020). Despite the inhomogeneity of the observations, point-by-point comparisons with model simulations that match the space and time of the observations are useful for studying key processes and mechanisms. Seasonality and long-term trends in the oceanic and polar ozone observations will be a focus of discussion in the forthcoming assessment (Sommariva et al., 2025).

Appendix A: Acronyms and abbreviations

Table A1. List of acronyms and abbreviations.

Acronym	Definition
ABLE-2B	Amazon Boundary Layer Experiment 2B
ABLE-3A/3B	Arctic Boundary Layer Experiment 3A/3B
ACCACIA	Aerosol–Cloud Coupling and Climate Interactions in the Arctic
ACE1	Aerosol Characterization Experiment 1
ACE-Asia	Aerosol Characterization Experiment – Asia
ACYSIS	Atmospheric Chemistry and Climate of the Southern Indian Ocean
ACTIVATE	Aerosol Cloud meTeorology Interactions oVer the western ATLantic Experiment
AEROSOLS99-INDOEX	Indian Ocean Experiment 1999
ARCPAC	Aerosol, Radiation, and Cloud Processes affecting Arctic Climate
ARCTAS	Arctic Research of the Composition of the Troposphere from Aircraft and Satellites
ATom	Atmospheric Tomography Mission
ATOMIC	Atlantic Tradewind Ocean–Atmosphere Mesoscale Interaction Campaign
BiPM	Bureau International des Poids et Mesures
CalNex	California Nexus
CAST	Coordinated Airborne Studies in the Tropics
CITE	Chemical Instrumentation Test and Evaluation
CLARIFY	Cloud–Aerosol–Radiation Interactions and Forcing: Year 2017
CN	Condensation Nuclei
CONTRAST	Convective Transport of Active Species in the Tropics
CSIRO	Commonwealth Scientific and Industrial Research Organisation
DISCOVER-AQ	Deriving Information on Surface Conditions from Column and Vertically Resolved Observations Relevant to Air Quality
DRAKE	Drake Passage cruise
DWD	Deutscher Wetterdienst
DYNAMO	Dynamics of the Madden–Julian Oscillation
EANET	Acid Deposition Monitoring Network in East Asia
ECC	Electrochemical concentration cell
FAAM	Facility for Airborne Atmospheric Measurements
GAW	Global Atmosphere Watch Programme
GRN	Global Research Network
HEGIFTOM	Harmonization and Evaluation of Ground-based Instruments for Free-Tropospheric Ozone Measurements
HIPPO	HIAPER Pole-to-Pole Observations
HURRICANE	Hurricane Field Campaign 2006
HYSPLIT	HYbrid Single-Particle Lagrangian Integrated Trajectory
ICEALOT	International Chemistry Experiment in the Arctic LOwer Troposphere
IGAC	International Global Atmospheric Chemistry project
IIOE2	Second International Indian Ocean Expedition
INTA	National Institute for Aerospace Technology
INTEX-B	Intercontinental Chemical Transport Experiment-B
INTEX-NA	Intercontinental Chemical Transport Experiment-North America
ITCT	Intercontinental Transport and Chemical Transformation
ITOP	Intercontinental Transport of Ozone and Precursors
KORUS-AQ	Korea-United States Air Quality Study
LCL	Last contact with land
MAGE	Marine Aerosol and Gas Exchange
Malaspina	Malaspina Circumnavigation Expedition
MOSAiC	Multidisciplinary drifting Observatory for the Study of Arctic Climate
MPI	Max Planck Institute
NAAMES	North Atlantic Aerosols and Marine Ecosystems Study

Table A1. Continued.

Acronym	Definition
NARE	North Atlantic Regional Experiment
NCEP	National Centers for Environmental Prediction
NEAQS	New England Air Quality Study
O-Buoy	Autonomous, ice-tethered buoy
ODEs	Ozone Depletion Events
PEM-Tropics	Pacific Exploratory Mission-Tropics
PEM-West	Pacific Exploratory Mission-West
POLARCAT	Polar Study using Aircraft, Remote Sensing, Surface Measurements and Models, of Climate, Chemistry, Aerosols, and Transport Research in the Tropics
RITS	
SAGA	Surface Ocean Lower Atmosphere Study
SEAC4RS	Studies of Emissions and Atmospheric Composition, Clouds and Climate Coupling by Regional Surveys
SOE	Southern Ocean Expedition
TAAF	Terres australes et antarctiques françaises
TEXAQS	Texas Air Quality Study
TOAR	Tropospheric Ozone Assessment Report
TORERO	Tropical Ocean tRoposphere Exchange of Reactive halogen species and Oxygenated VOC
TRACE-A	Transport and Atmospheric Chemistry near the Equator–Atlantic
TRACE-P	Transport and Chemical Evolution over the Pacific
VOCALS	VAMOS Ocean–Cloud–Atmosphere–Land Study
WACS	Western Atlantic Climate Study
WINTERSTORMS	Winter Storms Field Campaigns
WOUDC	World Ozone and Ultraviolet Radiation Data Centre
YES-AQ	YEllow Sea-Air Quality

Supplement. The supplement related to this article is available online at <https://doi.org/10.5194/essd-17-4901-2025-supplement>.

Author contributions. RS, ASL, and YK designed the study and led the data collection, assisted by TKK, AMaz, JEJ, SM, IEG, AMah, GC, WG, JCGM, KR, and MR. YK, FT, YI, HT, KK, JEJ, ASL, AC, PT, SM, IEG, RV, AMah, JS, HA, BB, MDS, DH, JG, ML, SCC, and IO carried out ship observations, collected data, and contributed to their quality control. JWH and PBS led the O-Buoy observations and contributed to the quality control of these data. RV, TKK, JL, DDP, JSH, TBR, IBP, EJW, BML, AJW, TC, FMF, JRS, IB, JP, CRT, RMStae, and AAA conducted aircraft observations, collected data, and contributed to data quality control. RVM, AMT, RMStau, DEK, JCGM, and MF performed ozonesonde observations, managed the data, and contributed to data quality control and homogenization. SM, IEG, WG, KS, JK, MNC, and MGS contributed to data collection from coastal/polar sites and the analysis of these data. MGS supervised the data collection and handling. MP contributed to data collection from surface sites. KCA and GC managed data and contributed to data curation, including quality assurance. KK and TKK performed filtering of the ship-based data and figure generation. AMaz, TKK, KR, MR, IEG, RS, ASL, and YK analyzed the dataset and prepared the figures and tables. YK drafted the manuscript. All of the co-authors reviewed manuscript the and contributed to revisions.

Competing interests. The contact author has declared that none of the authors has any competing interests.

Disclaimer. Publisher's note: Copernicus Publications remains neutral with regard to jurisdictional claims made in the text, published maps, institutional affiliations, or any other geographical representation in this paper. While Copernicus Publications makes every effort to include appropriate place names, the final responsibility lies with the authors.

Special issue statement. This article is part of the special issue “Tropospheric Ozone Assessment Report Phase II (TOAR-II) Community Special Issue (ACP/AMT/BG/ESSD/GMD inter-journal SI)”. It is a result of the Tropospheric Ozone Assessment Report, Phase II (TOAR-II, 2020–2024).

Acknowledgements. We acknowledge the NSF, UCAR/NCAR, NASA, NOAA (PMEL, CSD), ECCC, EANET, JAMSTEC, and NERC for funding and data management. With respect to the R/V *Mirai* cruises, we gratefully acknowledge the assistance from the principal investigators (PIs) and staff members of all cruises and the support from Global Ocean Development Inc. and Nippon Marine Enterprise, Ltd. The authors thank the IN MAP-IO support team of the OSU-R and OMP for data from the *Marion Dufresne*. Peter Winkler, Marian de Reus, Jos Lelieveld, Jonathan Williams, and Horst Fischer are acknowledged for the DWD-MPI dataset. We acknowledge the use of the CSIRO Marine National Facility (<https://ror.org/01mae9353>, last access: 6 September 2025) in undertaking this research on R/V *Investigator*. The finalized data will be available from the CSIRO Data Access Portal (DAP) with an accompanying DOI. Paty Matrai, Jan Bottemheim, and Bill Simpson are acknowledged for the O-Buoy data. The FAAM airborne

data were obtained using the BAe 146-301 atmospheric research aircraft (ARA) flown by Airtask Ltd and managed by the FAAM Airborne Laboratory, jointly operated by UKRI and the University of Leeds. The HEGIFTOM homogenized ozonesonde data are from PIs David Tarasick, Peter von der Gathen, Nis Jepsen, Rigel Kivi, Bryan Johnson, and Terry Deshler. The WOUDC ozonesonde data are from the Finnish Meteorological Institute – National Meteorological Service of Argentina, Australian Bureau of Meteorology, and Japan Meteorological Agency (JMA) and were retrieved from the WOUDC site (<https://wofdc.org/>, last access: 6 September 2025). The ozonesonde sounding campaign from the research vessel *Shoyo-Maru* was conducted as part of the project “Soundings of Ozone and Water in the Equatorial Region” (SOWER) in collaboration with the Japan Fisheries Agency. Regarding the data from Kennaook/Cape Grim, the Australian Bureau of Meteorology, who own and manage the station, and the CSIRO, who produced the dataset, are acknowledged. We gratefully acknowledge the NOAA Air Resources Laboratory (ARL) for providing the HYSPLIT transport model (<https://www.arl.noaa.gov/hysplit/>, last access: 23 November 2024). We also acknowledge NDACC, HEGIFTOM, and SHADOZ (<https://doi.org/10.57721/SHADOZ-V06>) for storing the original ozonesonde data. The ozone data from the Belgrano station would not have been possible without the collaboration agreement between INTA and National Antarctic Direction (DNA)/Argentinian Antarctic Institute (IAA) and the work done by the different technicians at Belgrano.

Financial support. This research has been supported by the Swiss Polar Institute (grant no. DIRCR-2018-004). Data collection was carried out as part of the international Multidisciplinary drifting Observatory for the Study of Arctic Climate (MOSAiC) expedition with the tag MOSAiC20192020, with activities supported by the *Polarstern* expedition AWI_PS122_00. The observations during the MOSAiC expedition were funded by the US National Science Foundation (grant nos. OPP 1807496, 1914781, and 1807163), the Swiss National Science Foundation (grant no. 200021_188478), the Swiss Polar Institute (grant no. DIRCR-2018-004), the Department of Energy Atmospheric System Research Program (grant no. DE-SC0019251), and the US National Oceanic and Atmospheric Administration (NOAA) Physical Sciences Laboratory. A subset of data were provided by the Atmospheric Radiation Measurement (ARM) user facility, a US Department of Energy Office of Science user facility managed by the Biological and Environmental Research program. Julia Schmale holds the Ingvar Kamprad chair for extreme environments research, sponsored by Ferring Pharmaceuticals. Matthew D. Shupe was supported by the DOE (grant no. DE-SC0021341) and NOAA cooperative agreement no. NA22OAR4320151. Ilana B. Pollack, Jeff Peischl, Chelsea R. Thompson, Ilann Bourgeois, and Brian M. Lerner were supported in part by NOAA cooperative agreement nos. NA17OAR4320101 and NA22OAR4320151. Detlev Helmig received funding from the US National Science Foundation, Interdisciplinary Biocomplexity in the Environment Program (project no. BE-IDEA 0410058), and from a grant from NOAA's Climate and Global Change Program (grant no. NA07OAR4310168). The TORERO (Tropical Ocean tRoposphere Exchange of Reactive halogen species and Oxygenated VOC) and CONTRAST (CONvective TRansport of Active Species

in the Tropics) projects were funded by the National Science Foundation (grant nos. AGS-1104104 and AGS-1261740). The involvement of the NSF-sponsored Lower Atmospheric Observing Facilities, managed and operated by the National Center for Atmospheric Research (NCAR) Earth Observing Laboratory (EOL) is acknowledged. This study was supported by the KAKENHI (grant no. 21H04933), the ArCS (Arctic Challenge for Sustainability; grant no. JPMXD1300000000) and ArCS II (grant no. JPMXD1420318865) of the Ministry of Education, Culture, Sports, Science, and Technology of Japan, the Specified Critical Technologies Research Promotion Grants from the Cabinet Office, Government of Japan, and by the Environmental Research and Technology Development Fund (ERTDF) from the Ministry of the Environment, Japan (grant nos. JPMEERF20252001 and JPMEERF24S12200). The O-buoy studies were supported by NSF award numbers 0612457, 1023118, 1023393, 1022834, and 1022773. Marios Panayi received support from the EMME-CARE project, funded by the European Union's Horizon 2020 Research and Innovation program (grant agreement no. 856612, with co-funding from the Government of Cyprus), and to the EU project AVENGERS (grant agreement no. 101081322). Data from Belgrano station has been partially funded by INTA and the Spanish Science Agency within the framework of the project GARDENIA (“Gases and aerosols in Antarctica: distribution, context and variability”, PID2021-122737NB-I00) and other former projects.

Review statement. This paper was edited by Luis Millan and reviewed by two anonymous referees.

References

- Abbatt, J. P. D., Leaitch, W. R., Aliabadi, A. A., Bertram, A. K., Blanchet, J.-P., Boivin-Rioux, A., Bozem, H., Burkart, J., Chang, R. Y. W., Charette, J., Chaubey, J. P., Christensen, R. J., Cirisan, A., Collins, D. B., Croft, B., Dionne, J., Evans, G. J., Fletcher, C. G., Galí, M., Ghahreman, R., Girard, E., Gong, W., Gosselin, M., Gourdal, M., Hanna, S. J., Hayashida, H., Herber, A. B., Hesarakci, S., Hoor, P., Huang, L., Hussherr, R., Irish, V. E., Keita, S. A., Kodros, J. K., Köllner, F., Kolonjari, F., Kunkel, D., Ladino, L. A., Law, K., Levasseur, M., Libois, Q., Liggio, J., Lizotte, M., Macdonald, K. M., Mahmood, R., Martin, R. V., Mason, R. H., Miller, L. A., Moravek, A., Mortenson, E., Mungall, E. L., Murphy, J. G., Namazi, M., Norman, A.-L., O'Neill, N. T., Pierce, J. R., Russell, L. M., Schneider, J., Schulz, H., Sharma, S., Si, M., Staebler, R. M., Steiner, N. S., Thomas, J. L., von Salzen, K., Wentzell, J. J. B., Willis, M. D., Wentworth, G. R., Xu, J.-W., and Yakobi-Hancock, J. D.: Overview paper: New insights into aerosol and climate in the Arctic, *Atmos. Chem. Phys.*, 19, 2527–2560, <https://doi.org/10.5194/acp-19-2527-2019>, 2019.
 ACP – Atmospheric Chemistry and Physics: POLARCAT (Polar Study using Aircraft, Remote Sensing, Surface Measurements and Models, of Climate, Chemistry, Aerosols, and Transport) special issue, https://acp.copernicus.org/articles/special_issue182.html (last access: 29 April 2025), 2015.
 Ahn, C., Yum, S. S., Park, M., Seo, P., Yoo, H.-J., Lee, M., and Lee, H.: Characteristics of new particle formation events occurred over the Yellow Sea in Spring-

- time from 2019 to 2022, *Atmos. Res.*, 308, 107510, <https://doi.org/10.1016/j.atmosres.2024.107510>, 2024.
- AMAP: AMAP Assessment 2021: Impacts of Short-lived Climate Forcers on Arctic Climate, Air Quality, and Human Health, AMAP – Arctic Monitoring and Assessment Programme, Tromsø, Norway, x + 375 pp., <https://www.apmap.no/documents/doc/amap-assessment-2021-impacts-of-short-lived-climate-forcers-on-arctic-climate-air-quality-and-human-health/3614> (last access: 10 September 2025), 2021.
- Angot, H., Blomquist, B., Howard, D., Archer, S., Bariteau, L., Beck, I., Boyer, M., Crotwell, M., Helmig, D., Hueber, J., Jacobi, H.-W., Jokinen, T., Kulmala, M., Lan, X., Laurila, T., Madronich, M., Neff, D., Petäjä, T., Posman, K., Quéléver, L., Shupe, M. D., Vimont, I., and Schmale, J.: Year-round trace gas measurements in the central Arctic during the MOSAiC expedition, *Sci. Data*, 9, 723, <https://doi.org/10.1038/s41597-022-01769-6>, 2022.
- Angot, H., Blomquist, B., Howard, D., Archer, S., Bariteau, L., Beck, I., Helmig, D., Hueber, J., Jacobi, H.-W., Jokinen, T., Laurila, T., Posman, K., Quéléver, L., Shupe, M. D., Schmale, J., and Boyer, M.: Ozone dry air mole fractions measured during MOSAiC 2019/2020 (merged dataset) [dataset], PANGAEA [data set], <https://doi.org/10.1594/PANGAEA.944393>, 2022b.
- Angot, H., Blomquist, B., Howard, D., Archer, S., Bariteau, L., Beck, I., Boyer, M., Helmig, D., Hueber, J., Jacobi, H.-W., Jokinen, T., Lan, X., Laurila, T., Madronich, M., Posman, K., Quéléver, L., Shupe, M. D., and Schmale, J.: Carbon monoxide dry air mole fractions measured during MOSAiC 2019/2020 (merged dataset) [dataset], PANGAEA [data set], <https://doi.org/10.1594/PANGAEA.944389>, 2022c.
- Barten, J. G. M., Ganzeveld, L. N., Steeneveld, G.-J., Blomquist, B. W., Angot, H., Archer, S. D., Bariteau, L., Beck, I., Boyer, M., von der Gathen, P., Helmig, D., Howard, D., Hueber, J., Jacobi, H.-W., Jokinen, T., Laurila, T., Posman, K. M., Quéléver, L., Schmale, J., Shupe, M. D., and Krol, M. C.: Low ozone dry deposition rates to sea ice during the MOSAiC field campaign: Implications for the Arctic boundary layer ozone budget, *Elementa*, 11, 00086, <https://doi.org/10.1525/elementa.2022.00086>, 2023.
- Bourgeois, I., Peischl, J., Thompson, C. R., Aikin, K. C., Campos, T., Clark, H., Commane, R., Daube, B., Diskin, G. W., Elkins, J. W., Gao, R.-S., Gaudel, A., Hintsa, E. J., Johnson, B. J., Kivi, R., McKain, K., Moore, F. L., Parrish, D. D., Querel, R., Ray, E., Sánchez, R., Sweeney, C., Tarasick, D. W., Thompson, A. M., Thouret, V., Witte, J. C., Wofsy, S. C., and Ryerson, T. B.: Global-scale distribution of ozone in the remote troposphere from the ATom and HIPPO airborne field missions, *Atmos. Chem. Phys.*, 20, 10611–10635, <https://doi.org/10.5194/acp-20-10611-2020>, 2020.
- Boylan, P., Helmig, D., and Oltmans, S.: Ozone in the Atlantic Ocean marine boundary layer, *Elementa*, 3, 000045, <https://doi.org/10.12952/journal.elementa.000045>, 2015.
- Chambers, S. D., Williams, A. G., Crawford, J., Griffiths, A. D., Krummel, P. B., Steele, L. P., Law, R. M., van der Schoot, M. V., Galbally, I. E., and Molloy, S. B.: A radon-only technique for characterising “baseline” constituent concentrations at Cape Grim, in: Baseline Atmospheric Program Australia 2011–2013, edited by: Derek, N., Krummel, P. B., and Cleland, S. J., Australian Bureau of Meteorology and CSIRO Marine and Atmospheric Research, <https://doi.org/10.25919/mp7r-1v15>, 2018.
- Chang, K.-L., Cooper, O. R., Gaudel, A., Petropavlovskikh, I., Effertz, P., Morris, G., and McDonald, B. C.: Technical note: Challenges in detecting free tropospheric ozone trends in a sparsely sampled environment, *Atmos. Chem. Phys.*, 24, 6197–6218, <https://doi.org/10.5194/acp-24-6197-2024>, 2024.
- Chiu, R., Obersteiner, F., Franchin, A., Campos, T., Bailey, A., Webster, C., Zahn, A., and Volkamer, R.: Intercomparison of fast airborne ozone instruments to measure eddy covariance fluxes: spatial variability in deposition at the ocean surface and evidence for cloud processing, *Atmos. Meas. Tech.*, 17, 5731–5746, <https://doi.org/10.5194/amt-17-5731-2024>, 2024.
- Coburn, S., Ortega, I., Thalman, R., Blomquist, B., Fairall, C. W., and Volkamer, R.: Measurements of diurnal variations and eddy covariance (EC) fluxes of glyoxal in the tropical marine boundary layer: description of the Fast LED-CE-DOAS instrument, *Atmos. Meas. Tech.*, 7, 3579–3595, <https://doi.org/10.5194/amt-7-3579-2014>, 2014.
- Dickerson, R. R., Rhoads, K. P., Carsey, T. P., Oltmans, S. J., Burrows, J. P., and Crutzen, P. J.: Ozone in the remote marine boundary layer: A possible role for halogens, *J. Geophys. Res.*, 104, 21385–21395, <https://doi.org/10.1029/1999JD900023>, 1999.
- Draxler, R. R. and Rolph, G. D.: HYSPLIT (HYbrid Single-Particle Lagrangian Integrated Trajectory), NOAA Air Resources Laboratory, College Park, MD, USA, <https://www.arl.noaa.gov/hysplit/hysplit/> (last access: 24 November 2024), 2013.
- EBAS: WMO Global Atmosphere Watch World data centres on aerosols and reactive gases, <https://ebas-data.nilu.no/> (last access: 29 April 2025), 2025.
- Fishman, J., Hoell Jr., J. M., Bendura, R. D., McNeal, R. J., and Kirchhoff, V. W. J. H.: NASA GTE TRACE A experiment (September–October 1992): Overview, *J. Geophys. Res.*, 101, 23865–23879, <https://doi.org/10.1029/96JD00123>, 1996.
- Forster, P., Storelvmo, T., Armour, K., Collins, W., Dufresne, J.-L., Frame, D., Lunt, D. J., Mauritsen, T., Palmer, M. D., Watanabe, M., Wild, M., and Zhang, H.: The Earth’s Energy Budget, Climate Feedbacks, and Climate Sensitivity, in: *Climate Change 2021: The Physical Science Basis, Contribution of Working Group I to the Sixth Assessment Report of the Intergovernmental Panel on Climate Change*, edited by: Masson-Delmotte, V., Zhai, P., Pirani, A., Connors, S. L., Péan, C., Berger, S., Caud, N., Chen, Y., Goldfarb, L., Gomis, M. I., Huang, M., Leitzell, K., Lonnoy, E., Matthews, J. B. R., Maycock, T. K., Waterfield, T., Yelekçi, O., Yu, R., and Zhou, B., Cambridge University Press, Cambridge, UK and New York, NY, USA, 923–1054, <https://doi.org/10.1017/9781009157896.009>, 2021.
- Fujiwara, M., Xie, S.-P., Shiotani, M., Hashizume, H., Hasebe, F., Vömel, H., Oltmans, S. J., and Watanabe, T.: Upper-tropospheric inversion and easterly jet in the tropics, *J. Geophys. Res.*, 108, 2796, <https://doi.org/10.1029/2003JD003928>, 2003.
- Galbally, I. E., Bentley, S. T., and Meyer, C. P.: Mid-latitude marine boundary layer ozone destruction at visible sunrise observed at Cape Grim, Tasmania, 41°S, *Geophys. Res. Lett.*, 27, 3841–3844, <https://doi.org/10.1029/1999GL010943>, 2000.
- Ganzeveld, L., Helmig, D., Fairall, C., Hare, J., and Pozzer, A.: Atmosphere-ocean ozone exchange: A global modeling study of biogeochemical, atmospheric, and waterside turbu-

- lence dependencies, *Global Biogeochem. Cy.*, 23, GB4021, <https://doi.org/10.1029/2008GB003301>, 2009.
- Gao, R. and Watts, L.: Ozone Dual Beam Spectrophotometer Volume Mixing Ratio Data – ICARTT format. Version 1.0, NSF NCAR Earth Observing Laboratory [data set], <https://doi.org/10.26023/150P-D7CG-310>, 2012.
- Gaudel, A., Bourgeois, I., Li, M., Chang, K.-L., Ziemke, J., Sauvage, B., Stauffer, R. M., Thompson, A. M., Kollonige, D. E., Smith, N., Hubert, D., Keppens, A., Cuesta, J., Heue, K.-P., Veefkind, P., Aikin, K., Peischl, J., Thompson, C. R., Ryerson, T. B., Frost, G. J., McDonald, B. C., and Cooper, O. R.: Tropical tropospheric ozone distribution and trends from in situ and satellite data, *Atmos. Chem. Phys.*, 24, 9975–10000, <https://doi.org/10.5194/acp-24-9975-2024>, 2024.
- Gómez Martín, J. C., Vömel, H., Hay, T. D., Mahajan, A. S., Ordóñez, C., Parrondo Sempere, M. C., Gil-Ojeda, M., and Saiz-Lopez, A.: On the variability of ozone in the equatorial eastern Pacific boundary layer, *J. Geophys. Res. Atmos.*, 121, 11086–11103, <https://doi.org/10.1002/2016JD025392>, 2016.
- Gong, W., Beagley, S. R., Toyota, K., Skov, H., Christensen, J. H., Lupu, A., Pendlebury, D., Zhang, J., Im, U., Kanaya, Y., Saiz-Lopez, A., Sommariva, R., Effertz, P., Halfacre, J. W., Jepsen, N., Kivi, R., Koenig, T. K., Müller, K., Nordstrøm, C., Petropavlovskikh, I., Shepson, P. B., Simpson, W. R., Solberg, S., Staebler, R. M., Tarasick, D. W., Van Malderen, R., and Vestenius, M.: Modelling Arctic Lower Tropospheric Ozone: processes controlling seasonal variations, EGUsphere [preprint], <https://doi.org/10.5194/egusphere-2024-3750>, 2025.
- Griffiths, P. T., Murray, L. T., Zeng, G., Shin, Y. M., Abraham, N. L., Archibald, A. T., Deushi, M., Emmons, L. K., Galbally, I. E., Hassler, B., Horowitz, L. W., Keeble, J., Liu, J., Moeini, O., Naik, V., O'Connor, F. M., Oshima, N., Tarasick, D., Tilmes, S., Turnock, S. T., Wild, O., Young, P. J., and Zanis, P.: Tropospheric ozone in CMIP6 simulations, *Atmos. Chem. Phys.*, 21, 4187–4218, <https://doi.org/10.5194/acp-21-4187-2021>, 2021.
- Halfacre, J. W., Knepp, T. N., Shepson, P. B., Thompson, C. R., Pratt, K. A., Li, B., Peterson, P. K., Walsh, S. J., Simpson, W. R., Matrai, P. A., Bottenheim, J. W., Netcheva, S., Perovich, D. K., and Richter, A.: Temporal and spatial characteristics of ozone depletion events from measurements in the Arctic, *Atmos. Chem. Phys.*, 14, 4875–4894, <https://doi.org/10.5194/acp-14-4875-2014>, 2014.
- Hardacre, C., Wild, O., and Emberson, L.: An evaluation of ozone dry deposition in global scale chemistry climate models, *Atmos. Chem. Phys.*, 15, 6419–6436, <https://doi.org/10.5194/acp-15-6419-2015>, 2015.
- Harris, J. M., Draxler, R. R., and Oltmans, S. J.: Trajectory model sensitivity to differences in input data and vertical transport method, *J. Geophys. Res.*, 110, D14109, <https://doi.org/10.1029/2004JD005750>, 2005.
- Harriss, R. C., Garstang, M., Wofsy, S. C., Beck, S. M., Bendura, R. J., Coelho, J. R. B., Drewry, J. W., Hoell Jr., J. M., Matson, P. A., McNeal, R. J., Molion, L. C. B., Navarro, R. L., Rabine, V., and Snell, R. L.: The Amazon Boundary Layer Experiment: Wet season 1987, *J. Geophys. Res.*, 95, 16721–16736, <https://doi.org/10.1029/JD095iD10p16721>, 1990.
- Harriss, R. C., Wofsy, S. C., Bartlett, D. S., Shipham, M. C., Jacob, D. J., Hoell Jr., J. M., Bendura, R. J., Drewry, J. W., McNeal, R. J., Navarro, R. L., Gidge, R. N., and Rabine, V. E.: The Arctic Boundary Layer Expedition (ABLE 3A): July–August 1988, *J. Geophys. Res.*, 97, 16383–16394, <https://doi.org/10.1029/91JD02109>, 1992.
- Harriss, R. C., Wofsy, S. C., Hoell Jr., J. M., Bendura, R. J., Drewry, J. W., McNeal, R. J., Pierce, D., Rabine, V., and Snell, R. L.: The Arctic Boundary Layer Expedition (ABLE-3B): July–August 1990, *J. Geophys. Res.*, 99, 1635–1643, <https://doi.org/10.1029/93JD01788>, 1994.
- Helming, D., Lang, E. K., Bariteau, L., Boylan, P., Fairall, C. W., Ganzeveld, L., Hare, J. E., Hueber, J., and Palandt, M.: Atmosphere-ocean ozone fluxes during the Tex-AQS 2006, STRATUS 2006, GOMECC 2007, GasEx 2008, and AMMA 2008 cruises, *J. Geophys. Res.-Atmos.*, 117, D04305, <https://doi.org/10.1029/2011JD015955>, 2012.
- Hoell, J. M., Davis, D. D., Liu, S. C., Newell, R., Shipham, M., Akimoto, H., McNeal, R. J., Bendura, R. J., and J. W. Drewry: Pacific Exploratory Mission-West A (PEM-West A): September–October 1991, *J. Geophys. Res.*, 101, 1641–1653, <https://doi.org/10.1029/95JD00622>, 1996.
- Hoell, J. M., Davis, D. D., Liu, S. C., Newell, R. E., Akimoto, H., McNeal, R. J., and Bendura, R. J.: The Pacific Exploratory Mission-West Phase B: February–March, 1994, *J. Geophys. Res.*, 102, 28223–28239, <https://doi.org/10.1029/97JD02581>, 1997.
- Hoell, J. M., Davis, D. D., Jacob, D. J., Rodgers, M. O., Newell, R. E., Fuelberg, H. E., McNeal, R. J., Raper, J. L., and Bendura, R. J.: Pacific Exploratory Mission in the tropical Pacific: PEM-Tropics A, August–September 1996, *J. Geophys. Res.*, 104(D5), 5567–5583, 1999.
- Hoell Jr., J. M., Davis, D. D., Gregory, G. L., McNeal, R. J., Bendura, R. J., Drewry, J. W., Barrick, J. D., Kirchhoff, V. W. J. H., Motta, A. G., Navarro, R. L., Dorko, W. D., and Owen, D. W.: Operational overview of the NASA GTE/CITE 3 airborne instrument intercomparisons for sulfur dioxide, hydrogen sulfide, carbonyl sulfide, dimethyl sulfide, and carbon disulfide, *J. Geophys. Res.*, 98, 23291–23304, <https://doi.org/10.1029/93JD00453>, 1993.
- Hu, X.-M., Sigler, J. M., and Fuentes, J. D.: Variability of ozone in the marine boundary layer of the equatorial Pacific Ocean, *J. Atmos. Chem.*, 66, 117–136, 2010.
- Inamdar, S., Tinel, L., Chance, R., Carpenter, L. J., Sabu, P., Chacko, R., Tripathy, S. C., Kerkar, A. U., Sinha, A. K., Bhaskar, P. V., Sarkar, A., Roy, R., Sherwen, T. T., Cuevas, C., Saiz-Lopez, A., Ram, K., and Mahajan, A. S.: Estimation of Reactive Inorganic Iodine Fluxes in the Indian and Southern Ocean Marine Boundary Layer, *Atmos. Chem. Phys.*, 20, 12093–12114, <https://doi.org/10.5194/acp-20-12093-2020>, 2020.
- Jacob, D. J., Crawford, J. H., Kleb, M. M., Connors, V. S., Bendura, R. J., Raper, J. L., Sachse, G. W., Gille, J. C., Emmons, L., and Heald, C. L.: Transport and Chemical Evolution over the Pacific (TRACE-P) aircraft mission: Design, execution, and first results, *J. Geophys. Res.*, 108, 9000, <https://doi.org/10.1029/2002JD003276>, 2003.
- Jacob, D. J., Crawford, J. H., Maring, H., Clarke, A. D., Dibb, J. E., Emmons, L. K., Ferrare, R. A., Hostetler, C. A., Russell, P. B., Singh, H. B., Thompson, A. M., Shaw, G. E., McCauley, E., Pederson, J. R., and Fisher, J. A.: The Arctic Research of the Composition of the Troposphere from Aircraft and Satellites (ARCTAS) mission: design, execution, and first results, At-

- mos. Chem. Phys., 10, 5191–5212, <https://doi.org/10.5194/acp-10-5191-2010>, 2010.
- JAMSTEC: R/V MIRAI MR17-05C Cruise Data, JAMSTEC [data set], <https://doi.org/10.17596/0001879>, 2017.
- JAMSTEC: R/V MIRAI MR17-08 Leg1 Cruise Data, JAMSTEC [data set], <https://doi.org/10.17596/0001881>, 2018a.
- JAMSTEC: R/V MIRAI MR17-08 Leg2 Cruise Data, JAMSTEC [data set], <https://doi.org/10.17596/0001882>, 2018b.
- JAMSTEC: R/V MIRAI MR18-04 Leg1 Cruise Data, JAMSTEC [data set], <https://doi.org/10.17596/0001886>, 2018c.
- JAMSTEC: R/V MIRAI MR18-04 Leg2 Cruise Data, JAMSTEC [data set], <https://doi.org/10.17596/0001887>, 2018d.
- JAMSTEC: R/V MIRAI MR18-05C Cruise Data, JAMSTEC [data set], <https://doi.org/10.17596/0001888>, 2018e.
- JAMSTEC: R/V MIRAI MR18-06 Leg1 Cruise Data, JAMSTEC [data set], <https://doi.org/10.17596/0001889>, 2019a.
- JAMSTEC: R/V MIRAI MR18-06 Leg4 Cruise Data, JAMSTEC [data set], <https://doi.org/10.17596/0001976>, 2019b.
- JAMSTEC: R/V MIRAI MR19-03C Cruise Data, JAMSTEC [data set], <https://doi.org/10.17596/0002077>, 2019c.
- JAMSTEC: R/V MIRAI MR19-04 Leg2 Cruise Data, JAMSTEC [data set], <https://doi.org/10.17596/0002101>, 2019d.
- JAMSTEC: R/V MIRAI MR19-04 Leg3 Cruise Data, JAMSTEC [data set], <https://doi.org/10.17596/0002118>, 2020a.
- JAMSTEC: R/V MIRAI MR20-E01 Cruise Data, JAMSTEC [data set], <https://doi.org/10.17596/0002152>, 2020b.
- JAMSTEC: R/V MIRAI MR20-05C Cruise Data, JAMSTEC [data set], <https://doi.org/10.17596/0002165>, 2020c.
- JAMSTEC: R/V MIRAI MR20-E02 Cruise Data, JAMSTEC [data set], <https://doi.org/10.17596/0002191>, 2020d.
- JAMSTEC: R/V MIRAI MR20-01 Cruise Data, JAMSTEC [data set], <https://doi.org/10.17596/0002121>, 2020e.
- JAMSTEC: R/V MIRAI MR21-01 Cruise Data, JAMSTEC [data set], <https://doi.org/10.17596/0002308>, 2021a.
- JAMSTEC: R/V MIRAI MR21-03 Cruise Data, JAMSTEC [data set], <https://doi.org/10.17596/0002310>, 2021b.
- JAMSTEC: R/V MIRAI MR21-05C Cruise Data, JAMSTEC [data set], <https://doi.org/10.17596/0002331>, 2021c.
- JURCAOS & JAMSTEC: R/V MIRAI MR21-06 Leg1 Cruise Data, JAMSTEC [data set], <https://doi.org/10.17596/0002312>, 2021,
- JURCAOS & JAMSTEC: R/V MIRAI MR21-06 Leg2 Cruise Data, JAMSTEC [data set], <https://doi.org/10.17596/0002313>, 2022.
- Johnson, J. E., Gammon, R. H., Larsen, J., Bates, T. S., Oltmans, S. J., and Farmer, J. C.: Ozone in the marine boundary layer over the Pacific and Indian Oceans: Latitudinal gradients and diurnal cycles, *J. Geophys. Res.*, 95, 11847–11856, <https://doi.org/10.1029/JD095iD08p11847>, 1990.
- Kanaya, Y., Miyazaki, K., Taketani, F., Miyakawa, T., Takashima, H., Komazaki, Y., Pan, X., Kato, S., Sudo, K., Sekiya, T., Inoue, J., Sato, K., and Oshima, K.: Ozone and carbon monoxide observations over open oceans on R/V *Mirai* from 67°S to 75°N during 2012 to 2017: testing global chemical reanalysis in terms of Arctic processes, low ozone levels at low latitudes, and pollution transport, *Atmos. Chem. Phys.*, 19, 7233–7254, <https://doi.org/10.5194/acp-19-7233-2019>, 2019.
- Kanaya, Y., Sommariva, R., Saiz-Lopez, A., Mazzeo, A., Koenig, T. K., Kawana, K., Johnson, J. E., Colomb, A., Tulet, P., Molloy, S., Galbally, I. E., Volkamer, R., Mahajan, A., Halfacre, J. W., Shepson, P. B., Schmale, J., Angot, H., Blomquist, B., Shupe, M., Helmig, D., Gil, J., Lee, M., Coburn, S. C., Ortega, I., Chen, G., Lee, J., Aikin, K. C., Parrish, D. D., Holloway, J. S., Ryerson, T. B., Pollack, I. B., Williams, E. J., Lerner, B. M., Weinheimer, A. J., Campos, T., Flocke, F. M., Spackman, J. R., Bourgeois, I., Peischl, J., Thompson, C. R., Staebler, R. M., Aliabadi, A. A., Gong, W., Van Malderen, R., Thompson, A. M., Stauffer, R. M., Kollonige, D. E., Gómez Martin, J. C., Fujiwara, M., Read, K., Rowlinson, M., Sato, K., Kurokawa, J., Iwamoto, Y., Taketani, F., Takashima, H., Navarro Comas, M., Panagi, M., and Schultz, M. G.: Observational ozone data over the global oceans and polar regions: The TOAR-II Oceans dataset version 2025, JAMSTEC [data set], <https://doi.org/10.17596/0004044>, 2025.
- Kleb, M. M., Chen, G., Crawford, J. H., Flocke, F. M., and Brown, C. C.: An overview of measurement comparisons from the INTEX-B/MILAGRO airborne field campaign, *Atmos. Meas. Tech.*, 4, 9–27, <https://doi.org/10.5194/amt-4-9-2011>, 2011.
- Law, K. S., Hjorth, J. L., Pernov, J. B., Whaley, C. H., Skov, H., Collaud Coen, M., Langner, J., Arnold, S. R., Tarasick, D., Christensen, J., Deushi, M., Effertz, P., Faluvegi, G., Gauss, M., Im, U., Oshima, N., Petropavlovskikh, I., Plummer, D., Tsigaridis, K., Tyro, S., Solberg, S., and Turnock, S. T.: Arctic tropospheric ozone trends, *Geophys. Res. Lett.*, 50, e2023GL103096, <https://doi.org/10.1029/2023GL103096>, 2023.
- Lelieveld, J., Van Aardenne, J., Fischer, H., De Reus, M., Williams, J., and Winkler, P.: Increasing ozone over the Atlantic Ocean, *Science*, 304, 1483–1487, 2004.
- Luhar, A. K., Woodhouse, M. T., and Galbally, I. E.: A revised global ozone dry deposition estimate based on a new two-layer parameterisation for air–sea exchange and the multi-year MACC composition reanalysis, *Atmos. Chem. Phys.*, 18, 4329–4348, <https://doi.org/10.5194/acp-18-4329-2018>, 2018.
- Mahajan, A. S., Tiné, L., Sarkar, A., Chance, R., Carpenter, L. J., Hulswar, S., Mali, P., Prakash, S., and Vinayachandran, P. N.: Understanding Iodine Chemistry over the Northern and Equatorial Indian Ocean, *J. Geophys. Res.-Atmos.*, 124, 8104–8118, <https://doi.org/10.1029/2018JD029063>, 2019.
- Monks, P. S., Carpenter, L. J., Penkett, S. A., Ayers, G. P., Gillett, R. W., Galbally, I. E., and Meyer, C. P.: Fundamental ozone photochemistry in the remote marine boundary layer: the SOAPEX experiment, measurement and theory, *Atmos. Environ.*, 32, 3647–3664, 1998.
- Nagao, I., Matsumoto, K., and Tanaka, H.: Sunrise ozone destruction found in the sub-tropical marine boundary layer, *Geophys. Res. Lett.*, 26, 3377–3380, 1999.
- NASA: MODIS/Terra Land Water Mask, NASA [data set], https://ldas.gsfc.nasa.gov/gldas/data/0.25deg/landmask_mod44w_025.asc (last access: 27 May 2019), 2019.
- Oltmans, S. J.: Surface ozone measurements in clean air, *J. Geophys. Res.*, 86, 1174–1180, <https://doi.org/10.1029/JC086iC02p01174>, 1981.
- Pan, L., Atlas, E., Salawitch, R., Honovich, S., Bresch, J., Randal, W., Apel, E., Hornbrook, R., Weinheimer, A., Anderson, D., Andrews, S., Baidar, S., Beaton, S., Campos, T., Carpenter, L., Chen, D., Dix, B., Donets, V., Hall, S., Hanisco, T., Homeyer, C., Huey, L., Jensen, J., Kaser, L., Kinnison, D., Koenig, T., Lamarque, J., Liu, C., Luo, J., Luo, Z., Montzka, D., Nicely, J., Pierce, R., Riemer, D., Robinson, T., Romashkin, P., Saiz-Lopez, A., Schaufler, S., Shieh, O., Stell, M., Ullmann, K., Vaughan, G., Volkamer, R. and Wolfe, G.: The Convective Transport of Ac-

- tive Species in the Tropics (CONTRAST) Experiment, *B. Am. Meteorol. Soc.*, 98, 106–128, <https://doi.org/10.1175/BAMS-D-14-00272.1>, 2017.
- Parrish, D. D., Millet, D. B., and Goldstein, A. H.: Increasing ozone in marine boundary layer inflow at the west coasts of North America and Europe, *Atmos. Chem. Phys.*, 9, 1303–1323, <https://doi.org/10.5194/acp-9-1303-2009>, 2009.
- Pollack, I. B., Lerner, B. T., and Ryerson, T. B.: Evaluation of ultra-violet light-emitting diodes for detection of atmospheric NO₂ by photolysis-chemiluminescence, *J. Atmos. Chem.*, 65, 111–125, <https://doi.org/10.1007/s10874-011-9184-3>, 2010.
- Pope, R. J., Kerridge, B. J., Siddans, R., Latter, B. G., Chipperfield, M. P., Feng, W., Pimplott, M. A., Dhomse, S. S., Retscher, C., and Rigby, R.: Investigation of spatial and temporal variability in lower tropospheric ozone from RAL Space UV-Vis satellite products, *Atmos. Chem. Phys.*, 23, 14933–14947, <https://doi.org/10.5194/acp-23-14933-2023>, 2023.
- Pound, R. J., Sherwen, T., Helmig, D., Carpenter, L. J., and Evans, M. J.: Influences of oceanic ozone deposition on tropospheric photochemistry, *Atmos. Chem. Phys.*, 20, 4227–4239, <https://doi.org/10.5194/acp-20-4227-2020>, 2020.
- Prados-Roman, C., Cuevas, C. A., Hay, T., Fernandez, R. P., Mahajan, A. S., Royer, S.-J., Galí, M., Simó, R., Dachs, J., Großmann, K., Kinnison, D. E., Lamarque, J.-F., and Saiz-Lopez, A.: Iodine oxide in the global marine boundary layer, *Atmos. Chem. Phys.*, 15, 583–593, <https://doi.org/10.5194/acp-15-583-2015>, 2015.
- Raper, J. L., Kleb, M. M., Jacob, D. J., Davis, D. D., Newell, R. E., Fuelberg, H. E., Bendura, R. J., Hoell, J. M., and McNeal, R. J.: Pacific Exploratory Mission in the Tropical Pacific: PEM-Tropics B, March–April 1999, *J. Geophys. Res.*, 106, 32401–32425, <https://doi.org/10.1029/2000JD900833>, 2001.
- Read, K. A., Mahajan, A. S., Carpenter, L. J., Evans, M. J., Faria, B. V. E., Heard, D. E., Hopkins, J. R., Lee, J. D., Moller, S. J., Lewis, A. C., Mendes, L., McQuaid, J. B., Oetjen, H., Saiz-Lopez, A., Pilling, M. J., and Plane, J. M. C.: Extensive halogen mediated ozone destruction over the tropical Atlantic Ocean, *Nature*, 453, 1232–1235, 2008.
- Ryerson, T. B., Buhr, M. P., Frost, G. J., Goldan, P. D., Holloway, J. S., Hübler, G., Jobson, B. T., Kuster, W. C., McKeen, S. A., Parrish, D. D., Roberts, J. M., Sueper, D. T., Trainer, M., Williams, J., and Fehsenfeld, F. C.: Emissions lifetimes and ozone formation in power plant plumes, *J. Geophys. Res.*, 103, 22569–22583, <https://doi.org/10.1029/98JD01620>, 1998.
- Saiz-Lopez, A. and von Glasow, R.: Reactive halogen chemistry in the troposphere, *Chem. Soc. Rev.*, 41, 6448–6472, 2012.
- Sarwar, G., Kang, D., Foley, K., Schwede, D., and Gantt, B.: Technical note: Examining ozone deposition over seawater, *Atmos. Environ.*, 141, 255–262, <https://doi.org/10.1016/j.atmosenv.2016.06.072>, 2016.
- Schröder, S., Schultz, M. G., Selke, N., Sun, J., Ahring, J., Mozaffari, A., Romberg, M., Epp, E., Lensing, M., Apweiler, S., Leufen, L. H., Betancourt, C., Hagemeyer, B., and Raalteveer, S.: TOAR Data Infrastructure, B2SHARE [data set], <https://doi.org/10.34730/4d9a287dec0b42f1aa6d244de8f19eb3>, 2024.
- Schultz, M. G., Schröder, S., Lyapina, O., Cooper, O. R., Galbally, I., Petropavlovskikh, I., von Schneidemesser, E., Tanimoto, H., Elshorbany, Y., Naja, M., Seguel, R. J., Dauert, U., Eckhardt, P., Feigenspan, S., Fiebig, M., Hjellbrekke, A.-G., Hong, Y.-D., Kjeld, P. C., Koide, H., Lear, G., Tarasick, D., Ueno, M., Wallasch, M., Baumgardner, D., Chuang, M.-T., Gillett, R., Lee, M., Molloy, S., Moolla, R., Wang, T., Sharps, K., Adame, J. A., Ancellet, G., Apadula, F., Artaxo, P., Barlasina, M. E., Bogucka, M., Bonasoni, P., Chang, L., Colomb, A., Cuevas, Agulló, E., Cupeiro, M., Degorska, A., Ding, A., Fröhlich, M., Frolova, M., Gadhami, H., Gheusi, F., Gilge, S., Gonzalez, M. Y., Gros, V., Hamad, S. H., Helmig, D., Henriques, D., Hermansen, O., Holla, R., Hueber, J., Im, U., Jaffe, D. A., Komala, N., Kubistin, D., Lam, K. -S., Laurila, T., Lee, H., Levy, I., Mazzoleni, C., Mazzoleni, L. R., McClure-Begley, A., Mohamad, M., Murovec, M., Navarro-Comas, M., Nicodim, F., Parrish, D., Read, K. A., Reid, N., Ries, L., Saxena, P., Schwab, J. J., Scorgie, Y., Senik, I., Simmonds, P., Sinha, V., Skorokhod, A. I., Spain, G., Spangl, W., Spoor, R., Springston, S. R., Steer, K., Steinbacher, M., Suharguniawan, E., Torre, P., Trickl, T., Weili, L., Weller, R., Xiaobin, X., Xue, L., and Zhiqiang, M.: Tropospheric Ozone Assessment Report: Database and metrics data of global surface ozone observations, *Elementa*, 5, 1582, <https://doi.org/10.1525/elementa.244>, 2017.
- Sekiya, T., Kanaya, Y., Sudo, K., Taketani, F., Iwamoto, Y., Aita, M. N., Yamamoto, A., and Kawamoto, K.: Global Bromine- and Iodine-Mediated Tropospheric Ozone Loss Estimated Using the CHASER Chemical Transport Model, *Sola*, 16, 220–227, <https://doi.org/10.2151/sola.2020-037>, 2020.
- Shiotani, M., Fujiwara, M., Hasebe, F., Hashizume, H., Vömel, H., Oltmans, S. J., and Watanabe, T.: Ozonesonde observations in the equatorial Eastern Pacific – the Shoyo-maru survey, *J. Meteorol. Soc. Jpn.*, 80, 897–909, <https://doi.org/10.2151/jmsj.80.897>, 2002.
- Shon, Z.-H., Madronich, S., Song, S.-K., Flocke, F. M., Knapp, D. J., Anderson, R. S., Shetter, R. E., Cantrell, C. A., Hall, S. R., and Tie, X.: Characteristics of the NO-NO₂-O₃ system in different chemical regimes during the MIRAGE-Mex field campaign, *Atmos. Chem. Phys.*, 8, 7153–7164, <https://doi.org/10.5194/acp-8-7153-2008>, 2008.
- Simpson, W. R., von Glasow, R., Riedel, K., Anderson, P., Ariya, P., Bottenheim, J., Burrows, J., Carpenter, L. J., Frieß, U., Goodsite, M. E., Heard, D., Hutterli, M., Jacobi, H.-W., Kaleschke, L., Neff, B., Plane, J., Platt, U., Richter, A., Roscoe, H., Sander, R., Shepson, P., Sodeau, J., Steffen, A., Wagner, T., and Wolff, E.: Halogens and their role in polar boundary-layer ozone depletion, *Atmos. Chem. Phys.*, 7, 4375–4418, <https://doi.org/10.5194/acp-7-4375-2007>, 2007.
- Simpson, W. R., Brown, S. S., Saiz-Lopez, A., Thornton, J. A., and Von Glasow, R.: Tropospheric halogen chemistry: sources, cycling, and impacts, *Chem. Rev.*, 115, 4035–4062, 2015.
- Singh, H. B., Brune, W. H., Crawford, J. H., Jacob, D. J., and Russell, P. B.: Overview of the summer 2004 Intercontinental Chemical Transport Experiment–North America (INTEX-A), *J. Geophys. Res.*, 111, D24S01, <https://doi.org/10.1029/2006JD007905>, 2006.
- Singh, H. B., Brune, W. H., Crawford, J. H., Flocke, F., and Jacob, D. J.: Chemistry and transport of pollution over the Gulf of Mexico and the Pacific: spring 2006 INTEX-B campaign overview and first results, *Atmos. Chem. Phys.*, 9, 2301–2318, <https://doi.org/10.5194/acp-9-2301-2009>, 2009.

- Sommariva, R., et al.: Tropospheric Ozone Assessment Report II: ozone distribution and variability in the oceanic and polar regions, in preparation, 2025.
- Stone, D., Sherwen, T., Evans, M. J., Vaughan, S., Ingham, T., Whalley, L. K., Edwards, P. M., Read, K. A., Lee, J. D., Moller, S. J., Carpenter, L. J., Lewis, A. C., and Heard, D. E.: Impacts of bromine and iodine chemistry on tropospheric OH and HO₂: comparing observations with box and global model perspectives, *Atmos. Chem. Phys.*, 18, 3541–3561, <https://doi.org/10.5194/acp-18-3541-2018>, 2018.
- Szopa, S., Naik, V., Adhikary, B., Artaxo, P., Berntsen, T., Collins, W. D., Fuzzi, S., Gallardo, L., Kiendler-Scharr, A., Klimont, Z., Liao, H., Unger, N., and Zanis, P.: Short-Lived Climate Forcers, in: Climate Change 2021: The Physical Science Basis, Contribution of Working Group I to the Sixth Assessment Report of the Intergovernmental Panel on Climate Change, edited by: Masson-Delmotte, V., Zhai, P., Pirani, A., Connors, S. L., Péan, C., Berger, S., Caud, N., Chen, Y., Goldfarb, L., Gomis, M. I., Huang, M., Leitzell, K., Lonnoy, E., Matthews, J. B. R., Maycock, T. K., Waterfield, T., Yelekçi, O., Yu, R., and Zhou, B., Cambridge University Press, Cambridge, UK and New York, NY, USA, 817–922, <https://doi.org/10.1017/9781009157896.008>, 2021.
- Thompson, A. M., Johnson, J. E., Torres, A. L., Bates, T. S., Kelly, L. C., Atlas, E., Greenberg, J. P., Donahue, N. M., Yvon, S. A., Saltzman, E. S., Heikes, B. G., Mosher, B. W., Shashkov, A. A., and Yegorov, V. I.: Ozone observations and a model of marine boundary layer photochemistry during SAGA 3, *J. Geophys. Res.*, 98, 16955–16968, <https://doi.org/10.1029/93JD00258>, 1993.
- TOAR-II Steering Committee: TOAR-II Community Special Issue Guidelines, https://igacproject.org/sites/default/files/2023-04/TOAR-II_Community_Special_Issue_Guidelines_202304.pdf (last access: 29 April 2025), 2023.
- Tulet, P., Van Baelen, J., Bosser, P., Brioude, J., Colomb, A., Goloub, P., Pazmino, A., Portafaix, T., Ramonet, M., Sellegri, K., Thyssen, M., Gest, L., Marquestaut, N., Mékiès, D., Metzger, J.-M., Athier, G., Blarel, L., Delmotte, M., Desprairies, G., Dournaux, M., Dubois, G., Duflot, V., Lamy, K., Gardes, L., Guillemot, J.-F., Gros, V., Kolasinski, J., Lopez, M., Magand, O., Noury, E., Nunes-Pinharanda, M., Payen, G., Pianezze, J., Picard, D., Picard, O., Prunier, S., Rigaud-Louise, F., Sicard, M., and Torres, B.: MAP-IO: an atmospheric and marine observatory program on board Marion Dufresne over the Southern Ocean, *Earth Syst. Sci. Data*, 16, 3821–3849, <https://doi.org/10.5194/essd-16-3821-2024>, 2024.
- Ueda, S., Iwamoto, Y., Taketani, F., Liu, M., and Matsui, H.: Morphological features and water solubility of iron in aged fine aerosol particles over the Indian Ocean, *Atmos. Chem. Phys.*, 23, 10117–10135, <https://doi.org/10.5194/acp-23-10117-2023>, 2023.
- Van Malderen, R., Thompson, A. M., Kollonige, D. E., Stauffer, R. M., Smit, H. G. J., Maillard Barras, E., Vigouroux, C., Petropavlovskikh, I., Leblanc, T., Thouret, V., Wolff, P., Effertz, P., Tarasick, D. W., Poyraz, D., Ancellet, G., De Backer, M.-R., Evan, S., Flood, V., Frey, M. M., Hannigan, J. W., Hernandez, J. L., Iarlori, M., Johnson, B. J., Jones, N., Kivi, R., Mahieu, E., McConville, G., Müller, K., Nagahama, T., Notholt, J., Piters, A., Prats, N., Querel, R., Smale, D., Steinbrecht, W., Strong, K., and Sussmann, R.: Global ground-based tropospheric ozone measurements: reference data and individual site trends (2000–2022) from the TOAR-II/HEGIFTOM project, *Atmos. Chem. Phys.*, 25, 7187–7225, <https://doi.org/10.5194/acp-25-7187-2025>, 2025.
- Volkamer, R., Baidar, S., Campos, T. L., Coburn, S., DiGangi, J. P., Dix, B., Eloranta, E. W., Koenig, T. K., Morley, B., Ortega, I., Pierce, B. R., Reeves, M., Sinreich, R., Wang, S., Zondlo, M. A., and Romashkin, P. A.: Aircraft measurements of BrO, IO, glyoxal, NO₂, H₂O, O₂–O₂ and aerosol extinction profiles in the tropics: comparison with aircraft-/ship-based in situ and lidar measurements, *Atmos. Meas. Tech.*, 8, 2121–2148, <https://doi.org/10.5194/amt-8-2121-2015>, 2015.
- Watanabe, K., Nojiri, Y., and Kariya, S.: Measurements of ozone concentrations on a commercial vessel in the marine boundary layer over the northern North Pacific Ocean, *J. Geophys. Res.*, 110, D11310, <https://doi.org/10.1029/2004JD005514>, 2005.
- Weinheimer, A.: NSF/NCAR GV HIAPER In Situ Chemiluminescence NO, NO₂, O₃ Data, Version 3.0, NSF NCAR Earth Observing Laboratory [data set], <https://doi.org/10.5065/D6PK0D6N>, 2015.
- Whaley, C. H., Law, K. S., Hjorth, J. L., Skov, H., Arnold, S. R., Langner, J., Pernov, J. B., Bergeron, G., Bourgeois, I., Christensen, J. H., Chien, R.-Y., Deushi, M., Dong, X., Effertz, P., Faluvegi, G., Flanner, M., Fu, J. S., Gauss, M., Huey, G., Im, U., Kivi, R., Marelle, L., Onishi, T., Oshima, N., Petropavlovskikh, I., Peischl, J., Plummer, D. A., Pozzoli, L., Raut, J.-C., Ryerson, T., Skeie, R., Solberg, S., Thomas, M. A., Thompson, C., Tsigaridis, K., Tsyro, S., Turnock, S. T., von Salzen, K., and Tarasick, D. W.: Arctic tropospheric ozone: assessment of current knowledge and model performance, *Atmos. Chem. Phys.*, 23, 637–661, <https://doi.org/10.5194/acp-23-637-2023>, 2023.
- Whittlestone, S., Gras, J. L., and Siems, S. T.: Surface air mass origins during the First Aerosol Characterization Experiment (ACE 1), *J. Geophys. Res.*, 103, 16341–16350, 1998.
- Wofsy, S. C., Daube, B. C., Jimenez, R., Kort, E., Pittman, J. V., Park, S., Commane, R., Xiang, B., Santoni, G., Jacob, D., Fisher, J., Pickett-Heaps, C., Wang, H., Wecht, K., Wang, Q.-Q., Stephens, B. B., Shertz, S., Watt, A. S., Romashkin, P., Campos, T., Haggerty, J., Cooper, W. A., Rogers, D., Beaton, S., Hendershot, R., Elkins, J. W., Fahey, D. W., Gao, R. S., Moore, F., Montzka, S. A., Schwarz, J. P., Perring, A. E., Hurst, D., Miller, B. R., Sweeney, C., Oltmans, S., Nance, D., Hintsa, E., Dutton, G., Watts, L. A., Spackman, J. R., Rosenlof, K. H., Ray, E. A., Hall, B., Zondlo, M. A., Diao, M., Keeling, R., Bent, J., Atlas, E. L., Lueb, R., and Mahoney, M. J.: HIPPO Merged 10-second Meteorology, Atmospheric Chemistry, and Aerosol Data, Version 1.0 (CDIAC Release 20121129/ NCAR EOL Version 1.0), UCAR/NCAR – Earth Observing Laboratory [data set], https://doi.org/10.3334/CDIAC/HIPPO_010, 2017.
- Wofsy, S. C., Afshar, S., Allen, H. M., Apel, E. C., Asher, E. C., Barletta, B., Bent, J., Bian, H., Biggs, B. C., Blake, D. R., Blake, N., Bourgeois, I., Brock, C. A., Brune, W. H., Budney, J. W., Bui, T. P., Butler, A., Campuzano-Jost, P., Chang, C. S., Chin, M., Commane, R., Correa, G., Crounse, J. D., Cullis, P. D., Daube, B. C., Day, D. A., Dean-Day, J. M., Dibb, J. E., DiGangi, J. P., Diskin, G. S., Dollner, M., Elkins, J. W., Erdesz, F., Fiore, A. M., Flynn, C. M., Froyd, K. D., Gesler, D. W., Hall, S. R., Hanisco, T. F., Hannun, R. A., Hills, A. J., Hintsa, E. J., Hoff-

man, A., Hornbrook, R. S., Huey, L. G., Hughes, S., Jimenez, J. L., Johnson, B. J., Katich, J. M., Keeling, R. F., Kim, M. J., Kupc, A., Lait, L. R., McKain, K., McLaughlin, R. J., Meinardi, S., Miller, D. O., Montzka, S. A., Moore, F. L., Morgan, E. J., Murphy, D. M., Murray, L. T., Nault, B. A., Neuman, J. A., Newman, P. A., Nicely, J. M., Pan, X., Paplawsky, W., Peischl, J., Prather, M. J., Price, D. J., Ray, E. A., Reeves, J. M., Richardson, M., Rollins, A. W., Rosenlof, K. H., Ryerson, T. B., Scheuer, E., Schill, G. P., Schroder, J. C., Schwarz, J. P., St. Clair, J. M., Steenrod, S. D., Stephens, B. B., Strode, S. A., Sweeney, C., Tanner, D., Teng, A. P., Thamess, A. B., Thompson, C. R., Ullmann, K., Veres, P. R., Wagner, N. L., Watt, A., Weber, R., Weinzierl, B. B., Wennberg, P. O., Williamson, C. J., Wilson, J. C., Wolfe, G. M., Woods, C. T., Zeng, L. H., and Vieznor, N.: ATom: Merged Atmospheric Chemistry, Trace Gases, and Aerosols, Version 2, ORNL DAAC, Oak Ridge, Tennessee, USA, <https://doi.org/10.3334/ORNLDAAC/1925>, 2021.

Young, P. J., Naik, V., Fiore, A. M., Gaudel, A., Guo, J., Lin, M. Y., Neu, J. L., Parrish, D. D., Rieder, H. E., Schnell, J. L., Tilmes, S., Wild, O., Zhang, L., Ziemke, J. R., Brandt, J., Delcloo, A., Doherty, R. M., Geels, C., Hegglin, M. I., Hu, L., Im, U., Kumar, R., Luhar, A., Murray, L., Plummer, D., Rodriguez, J., Saiz-Lopez, A., Schultz, M. G., Woodhouse, M. T. and Zeng, G.: Tropospheric Ozone Assessment Report: Assessment of global-scale model performance for global and regional ozone distributions, variability, and trends, *Elem. Sci. Anth.*, 6, 10, <https://doi.org/10.1525/elementa.265>, 2018.

Zhang, B., Liu, H., Crawford, J. H., Chen, G., Fairlie, T. D., Chambers, S., Kang, C.-H., Williams, A. G., Zhang, K., Considine, D. B., Sulprizio, M. P., and Yantosca, R. M.: Simulation of radon-222 with the GEOS-Chem global model: emissions, seasonality, and convective transport, *Atmos. Chem. Phys.*, 21, 1861–1887, <https://doi.org/10.5194/acp-21-1861-2021>, 2021.